aerospace

MDPI

Article

Danuri's Two-Year Orbit Maintenance and Maneuver Recovery in a Low Lunar Polar Orbit: Flight Dynamics Results and Operational Lessons

Jonghee Bae [1], Jun Bang [1], SeungBum Hong [1] and Young-Joo Song [2,3,4,*]

[1] Satellite & Space Exploration Research Directorate, Korea Aerospace Research Institute, Daejeon 34133, Republic of Korea; jbae@kari.re.kr (J.B.); bj1545@kari.re.kr (J.B.); sbhong@kari.re.kr (S.H.)
[2] School of Space Research, Kyung Hee University, Yongin 17104, Republic of Korea
[3] G-LAMP NEXUS Institute, Kyung Hee University, Yongin 17104, Republic of Korea
[4] Department of Astronomy and Space Science, Kyung Hee University, Yongin 17104, Republic of Korea
* Correspondence: dearyjs@khu.ac.kr

Abstract

The Korea Pathfinder Lunar Orbiter (KPLO), "Danuri," conducted orbit maintenance during its two-year mission in a near-circular 100 km low lunar polar orbit. Since entering its mission orbit in January 2023, Orbit Maintenance Maneuvers (OMMs) were required to compensate for lunar perturbations, particularly the non-uniform lunar gravitational field. Over two years, 13 OMM pairs, each consisting of OMM-a and OMM-b burns, were executed through an integrated process of Orbit Determination (OD), Maneuver Planning (MP), and Maneuver Recovery (MR). Because onboard acceleration measurements were unavailable, maneuver performance was reconstructed from NASA's Deep Space Network (DSN) tracking data using post-maneuver OD and targeter-based MR with thruster modeling. The preliminary and final OD solutions used for MP maintained uncertainties of several tens of meters in position and a few centimeters per second in velocity. Under Danuri's operational conditions, reliable preliminary maneuver performance estimates could be obtained using tracking data collected within approximately 2–4 h after maneuver execution. Subsequent targeter-based MR enabled maneuver-performance reconstruction and iterative thrust-efficiency calibration, yielding an average reconstructed performance of approximately 99%. OMM planning was also adapted in two conjunction-risk cases while preserving orbit-maintenance objectives. These flight results validate a ground-based closed-loop OD–MP–MR framework for reliable low lunar orbit maintenance and maneuver-performance reconstruction without onboard acceleration measurements.

Keywords: Korea Pathfinder Lunar Orbiter; Danuri; orbit maintenance; flight dynamics operation; orbit determination; Maneuver Planning; maneuver recovery

Academic Editors: Eloy Peña-Asensio, Anna Mittelholz, Wajiha Iqbal, Ariel N. Deutsch

Received: 7 October 2026
Revised: 20 November 2026
Accepted: 21 November 2026
Published: 24 November 2026

Copyright: © 2026 by the authors. Licensee MDPI, Basel, Switzerland. This article is an open access article distributed under the terms and conditions of the Creative Commons Attribution (CC BY) license.

1. Introduction

In recent years, lunar exploration has experienced a significant resurgence, driven by both national space agencies and private enterprises aiming to advance scientific understanding and establish a sustained human and robotic presence on the Moon. Major governmental programs include NASA Artemis [1], which targets a return of humans to the lunar surface, as well as China's Chang'e program [2–4], India's Chandrayaan missions

[5], and Japan's SLIM [6], all of which have successfully demonstrated robotic exploration capabilities. Concurrently, private-sector missions such as Astrobotic's Peregrine Lander [7], Japan's ispace program [8], and Israel's SpaceIL [9] have marked the emergence of commercial participation in lunar exploration. Collectively, these efforts are accelerating advancements in lunar science, including investigations of surface geology, resource potential, and environmental conditions, while fostering the development of technologies essential for long-term space exploration.

With growing global interest in lunar exploration, KPLO, also known as Danuri (which means "enjoy everything on the Moon" in Korean), is South Korea's first lunar exploration mission. Launched on 4 August 2022, from Cape Canaveral Space Force Station aboard a SpaceX Falcon 9, Danuri followed a BLT trajectory and entered lunar orbit on 27 December 2022, after three LOI maneuvers [10,11]. Following a one-month commissioning phase to verify spacecraft subsystems and payload performance, Danuri began nominal science operations. Official mission-orbit numbering, however, began on 1 January 2023. Danuri carries six scientific and technological payloads: LUTI for high-resolution imaging of potential landing sites [12], PolCam for surface texture and regolith studies [13], NASA-developed SHC for observing permanently shadowed regions to detect water ice [14], KMAG for lunar magnetic-field measurements [15], KGRS for surface elemental analysis [16], and DTN for testing interplanetary internet protocols [17]. Further details of the spacecraft bus, subsystems, and payload accommodation are provided in Ref. [18]. By March 2026, Danuri had completed more than 14,000 lunar orbits, established approximately 7378 communication contacts with NASA's DSN and the KDSA, and processed 64,113 observation requests for LUTI, PolCam, and SHC into observation plans. Its five scientific payloads had returned 9311 GiBytes of data, subsequently delivered to the payload teams for analysis. These activities have advanced lunar science and Korea's deep-space exploration capabilities, with scientific data progressively released through the public KPDS repository. Figure 1 shows Tycho Crater in the Moon's southern highlands, imaged by LUTI on 26 September 2023.

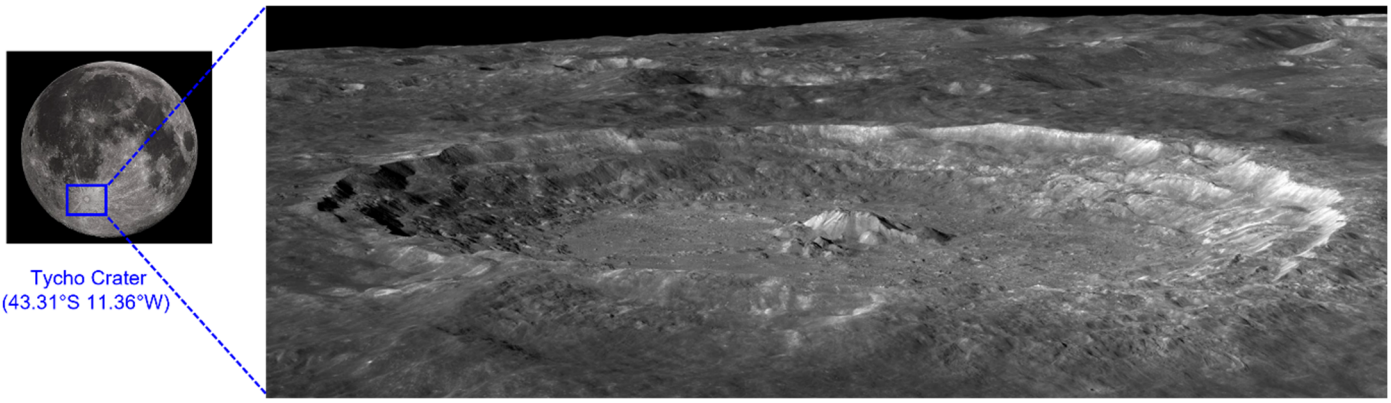


Figure 1. Tycho Crater captured by LUTI, one of Danuri's payloads, on 26 September 2023. (credit: KARI).

Following the successful completion of its one-year primary mission in January 2024, Danuri entered an extended mission phase, continuing operations in its nominal orbit until February 2025, with a subsequent extended mission planned under modified orbital conditions. The long-term acquisition of high-quality scientific data critically depends on the precise maintenance of orbital parameters, which is achieved through OMMs. Over a two-year period, Danuri executed a total of 13 OMMs, each consisting of paired maneuvers, at intervals of approximately two months, ensuring compliance with mission orbit requirements and enabling consistent scientific observations. Successful execution of

OMMs requires high-precision OD, accurate MP, reliable prediction of thruster performance, and rigorous post-maneuver evaluation through MR.

Accurate assessment of maneuver execution performance is essential because the post-maneuver orbit serves as the initial condition for subsequent orbit prediction, mission-orbit compliance evaluation, and future MP. This assessment is also closely related to conjunction assessment and mitigation planning, since a small discrepancy between the planned and realized maneuver can alter the predicted relative geometry with other lunar orbiters. In real-flight operations, however, OMM performance cannot be evaluated solely from planned maneuver commands. The actual maneuver outcome is affected by thruster performance uncertainty, attitude-pointing error, finite-burn implementation, execution timing error, and OD uncertainty. These effects are particularly important for low lunar orbiters because even small maneuver errors can accumulate rapidly under the perturbed lunar dynamical environment and can lead to deviations from the required periapsis and apoapsis altitude bounds. For this reason, MR is essential for estimating the effective maneuver performance after execution and for updating subsequent MP and OD strategies. A further operational challenge arises when a spacecraft does not carry onboard acceleration measurement capability or when such information is not available for direct maneuver reconstruction. In such cases, the actual maneuver performance cannot be directly reconstructed from onboard acceleration measurements, and the FD team must instead recover the maneuver effect indirectly from pre- and post-maneuver OD solutions and orbit-prediction residuals relative to the planned maneuver profile. This constraint makes the operational process more complex, because maneuver evaluation becomes tightly coupled with OD quality that is strongly affected by tracking-data coverage, and the modelling accuracy of MP. Therefore, a systematic and flight-proven procedure for maneuver recovery without onboard acceleration measurements is valuable for future low lunar orbit missions, particularly for small or cost-constrained spacecraft that may not include dedicated acceleration sensors.

While orbit maintenance strategies for lunar missions have been addressed in previous studies, detailed flight-based accounts of the complete operational workflow under limited onboard measurement conditions remain limited. Earlier works, including those on Lunar Prospector [19], SELENE [20], LADEE [21,22], and LRO [23–25], have reported maneuver performance, OD results, and operational experience. Detailed MP and recovery procedures for LADEE [26] and long-term operational adaptations for LRO [27] have also been documented. Nevertheless, further flight-based insight is needed into how planning, execution, and recovery processes are integrated into a complete operational workflow when onboard acceleration measurements are unavailable. Furthermore, the impact of unplanned operational constraints, such as conjunction avoidance with other lunar orbiters, is rarely discussed in the context of this complete OD–MP–MR workflow. Although conjunction-related modifications to orbit-maintenance plans have been reported for CH2O [28], the present study examines how such constraints were accommodated within Danuri's integrated FD operational workflow. The limited availability of such integrated operational accounts presents challenges for mission designers and operators seeking practical guidance on orbit maintenance and maneuver recovery without onboard acceleration measurements. Accordingly, the main technical gap addressed in this paper is not merely the analysis of OMM execution results, but the formulation and validation of an operational framework that can maintain a low lunar mission orbit and recover maneuver performance under limited onboard measurement conditions. By using Danuri's two-year flight experience, this study provides a unique real-mission case in which OMM planning, post-maneuver OD, MR, and operational replanning were repeatedly conducted in an integrated manner. This perspective distinguishes the present work from conventional orbit-maintenance summaries and highlights its relevance to future lunar orbiters that must

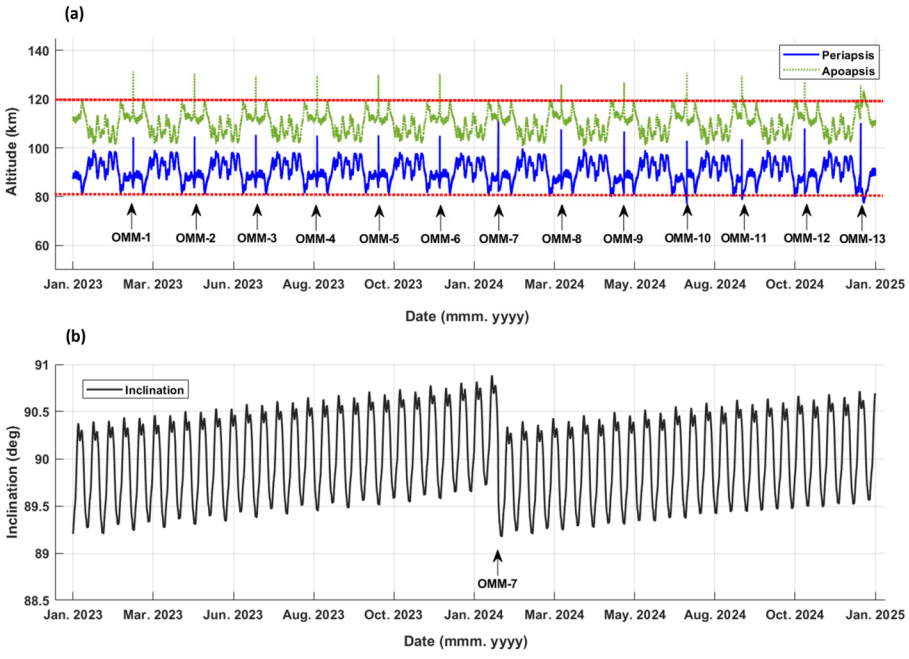
achieve reliable operations with constrained spacecraft resources and limited onboard diagnostic capability.

The remainder of this paper is organized as follows. Section 2 describes the Danuri mission orbit. Section 3 presents the OMM methodology, including orbit-maintenance strategy, OD configuration, MR approach, and the operational workflow. Section 4 presents the flight results, with emphasis on OD performance, MP results, conjunction-risk-related planning cases, and MR-based maneuver-performance reconstruction. Section 5 discusses operational lessons and implications derived from the two-year flight experience. Finally, Section 6 summarizes the conclusions.

2. Mission Orbit Overview

Danuri successfully completed two years of lunar mission operations, maintaining a circular polar orbit with a mean altitude of 100 km and an altitude dead band of ±20 km during the nominal and first extended mission phases. The mission required maintaining the mean orbital inclination of 90 ± 0.25 degrees to satisfy the scientific objectives. Initially, the allowable altitude dead band was set at ±30 km; however, it was later reduced to ±20 km at the request of the SHC team to enhance imaging performance. This adjustment was thoroughly evaluated in terms of fuel consumption, operational feasibility, and potential impacts on other payloads, and was subsequently approved. Following the successful completion of its primary one-year mission in January 2024, Danuri entered the first extended mission phase, continuing operations within the same orbital configuration. As of February 2025, the spacecraft had successfully maintained the required orbit throughout the two-year operational period.

Figure 2 presents the planned altitude and inclination variations during the two-year operation. Figure 2a shows the periapsis and apoapsis altitude variations, while Figure 2b illustrates the inclination variations. As shown in Figure 2b, OMM-7 was planned and executed as an inclination correction maneuver to restore the inclination trend and ensure compliance with the inclination requirement of 90 ± 0.25 degrees during the second year of the lunar mission. It should be noted that the inclination shown in Figure 2b represents the osculating inclination, whereas the mission requirement of 90 ± 0.25° was applied to the mean inclination throughout the two-year operational period.



https://doi.org/10.3390/aerospace13121107

Figure 2. Planned altitude and inclination variations over Danuri's two-year operation. (**a**) Periapsis and apoapsis altitude variations. (**b**) Osculating inclination variation, including the OMM-7 inclination correction.

The analysis in this study is limited to the nominal and first extended mission phases shown in Figure 2. After this period, following a reassessment of the spacecraft status, remaining propellant, and inputs from the science PIs, Danuri transitioned to a 60 ± 30 km low lunar orbit in February 2025 and subsequently to a frozen-orbit configuration in September 2025 to further enhance scientific return while minimizing propellant consumption. A more detailed description of the mission selection process and orbital characteristics for Danuri's extended mission operations is provided in Ref. [29].

3. OMM Methods

3.1. OMM Design Strategy

3.1.1. Dynamic Model and Maneuver Representation

Danuri's OMM strategy was established by propagating the long-term evolution of a low lunar polar orbit using a high-fidelity dynamic model, as follows [30].

$$\dot{\mathbf{r}} = \mathbf{v}, \tag{1}$$

$$\dot{\mathbf{v}} = -\frac{\mu_M}{r^3}\mathbf{r} + \mathbf{a}_{\mathrm{G}} + \mathbf{a}_{\mathrm{E}} + \mathbf{a}_{\mathrm{S}} + \mathbf{a}_{\mathrm{SRP}} + \mathbf{a}_{\mathrm{LRP}} + \mathbf{a}_{\mathrm{OMM}}, \tag{2}$$

where $\mathbf{r}$ and $\mathbf{v}$ are the spacecraft position and velocity vectors with respect to the Moon, μ_M is the lunar gravitational parameter. The acceleration terms $\mathbf{a}_{\mathrm{G}}$, $\mathbf{a}_{\mathrm{E}}$, $\mathbf{a}_S$, $\mathbf{a}_{\mathrm{SRP}}$, $\mathbf{a}_{\mathrm{LRP}}$, and $\mathbf{a}_{\mathrm{OMM}}$ denote the perturbations due to non-spherical lunar gravity, the Earth, the Sun, solar radiation pressure, lunar albedo and thermal radiation pressure, and OMM thrust, respectively. The lunar albedo and thermal radiation pressure were represented using the simplified reflection model summarized in Table 1. The OMM acceleration term was modeled as a finite burn generated by Danuri's ACT system. Each OMM used four ACTs, each providing 3.49 N of thrust with an Isp of 218.94 s, and the approximately 15 deg cant angle of the ACT installation was reflected in the thruster modeling to represent the effective thrust direction and acceleration [29]. Table 1 summarizes the dynamic, numerical integration, and maneuver modeling settings used for Danuri's OMM-related flight-dynamics operations. Using this dynamic model, the natural evolution of mission orbit was analyzed to determine when and how OMMs should be applied to maintain the prescribed altitude dead band. For MP, a degree and order of 150 × 150 (shown in Table 1) were used to limit accumulated truncation effects when predicting the e–ω evolution over approximately two months. This choice was informed by a preliminary study conducted before Danuri's launch to examine the effects of lunar gravity-field truncation on orbit propagation [31].

Table 1. Summary of the dynamic and maneuver modelling settings used for Danuri's OMM flight operations.

Category	Applied Setting
Central body	Moon
Planetary ephemeris	JPL DE430
Third-body perturbations	Earth and Sun
Lunar gravity field	GL0660B, 150 × 150
Solar radiation pressure	Spherical spacecraft model

Shadow model	Dual-cone shadow model considering Earth and Moon occultation
Albedo and thermal radiation pressure	Simplified reflection model
Numerical integrator	7th–8th order Runge–Kutta integrator with variable step-size control
Integration step-size control	Phase-dependent maximum step size for general propagation and thruster-firing phases
Maneuver model	Finite-burn model reflecting the in-flight maneuver modeling characteristics used for Danuri (3.49 N of thrust with 218.94 s Isp for each ACT)

3.1.2. e–ω Based Paired-Maneuver Strategy

Due to the non-uniform lunar gravitational field, the periapsis altitude of a spacecraft in a low lunar orbit decreases over time in the absence of orbit maintenance maneuver, ultimately leading to surface impact if left uncorrected. For example, a spacecraft in a circular polar orbit at an altitude of 100 km is expected to impact the lunar surface within approximately 6~7 months, as gravitational perturbations from the Moon, Earth, and Sun progressively increase orbital eccentricity [32]. To mitigate this effect, Danuri performed periodic OMMs to regulate the eccentricity (e) and argument of periapsis (ω), thereby controlling the long-term evolution of the orbit. This e-ω phase-space interpretation is consistent with previous low-lunar-orbit stationkeeping studies, including LP [33,34], SELENE [20], and LRO [23–25], in which repeated e-ω patterns were used to satisfy altitude-control requirements. In terms of eccentricity-vector evolution, the e-ω state can be expressed using two in-plane components [35]:

$$C = e\cos\omega, \qquad S = e\sin\omega \tag{3}$$

where C and S define the eccentricity vector in the orbital plane. In this representation, the magnitude of the vector corresponds to the orbital eccentricity, while its direction represents the argument of periapsis. Therefore, a maneuver-induced change in the e-ω phase space can be interpreted as a translation of the eccentricity vector. The required translation from the current state (e_i, ω_i) to the desired post-maneuver state (e_0, ω_0) can be written as:

$$\Delta e_\omega = \sqrt{(e_0 cos\omega_0 - e_i cos\omega_i)^2 + (e_0 sin\omega_0 - e_i sin\omega_i)^2} \tag{4}$$

where Δe_ω represents the magnitude of the eccentricity-vector shift in the e-ω plane. Using this interpretation, Danuri's paired OMMs can be understood as controlled translations of the eccentricity vector to a region where the subsequent natural evolution remains within the allowable altitude boundary. This e-ω based strategy was directly connected to the mission requirement of maintaining the 100 km ± 20 km altitude dead band during the nominal and first extended mission phases.

For Danuri, the OMM strategy was implemented as a pair of maneuvers separated by approximately half an orbital period. An acceleration maneuver near apoapsis was performed to increase the periapsis altitude, followed by a deceleration maneuver near periapsis to reduce the apoapsis altitude. This paired maneuver concept allowed the orbit to be adjusted while keeping both the periapsis and apoapsis altitudes within the mission-required altitude dead band. Several approaches are available for achieving such altitude control. Periodic circularization and altitude-triggered corrections are among the alternatives examined in pre-launch KPLO studies [32]. Simple implementations of these approaches can require frequent maneuvers to maintain the prescribed 100 km ± 20 km altitude band. By selecting an appropriate post-maneuver e–ω state, the adopted strategy can use natural orbital evolution to keep the orbit within the allowable altitude band for two

months or longer. This reduces the frequency of orbit-maintenance operations, the associated interruptions to science observations, and the operational workload. For the required orbital correction, a single impulse at a selected location provides limited flexibility to achieve the target semi-major axis, eccentricity, and argument of periapsis simultaneously. Paired maneuvers in the velocity and anti-velocity directions were therefore used to provide the required orbital adjustment. The strategy was selected primarily to satisfy the altitude constraints while reducing maneuver frequency and operational interruptions, rather than on the basis of a demonstrated minimum-total-ΔV solution over a specified maintenance interval.

For each maneuver campaign, however, the actual delta-V delivered by each OMM burn could not be directly measured because Danuri was not equipped with an onboard accelerometer. This limitation necessitated precise pre-MP and rigorous post-MR. Therefore, the OMM strategy required not only accurate maneuver design before execution but also post-maneuver OD to estimate the actual maneuver performance and update the subsequent MP, which made the FD operation procedure more complex and time-consuming during real-flight operations. Figure 3 illustrates an example of the e–ω evolution during the fifth OMM (OMM-5), where the altitude dead band is effectively maintained through the paired maneuvers OMM-5a and OMM-5b. As shown in the figure, OMM-5a and OMM-5b move the spacecraft state along the e–ω phase space in a controlled manner, preventing the orbit from evolving outside the allowable altitude boundary. This example demonstrates how the e-*ω* based stationkeeping concept was implemented as an actual paired-maneuver sequence during Danuri's flight operations. The transformation of this concept into executable maneuver plans, including targeting setup, control-parameter refinement, and the TDS–FDS operational interface, is discussed in Section 3.4.

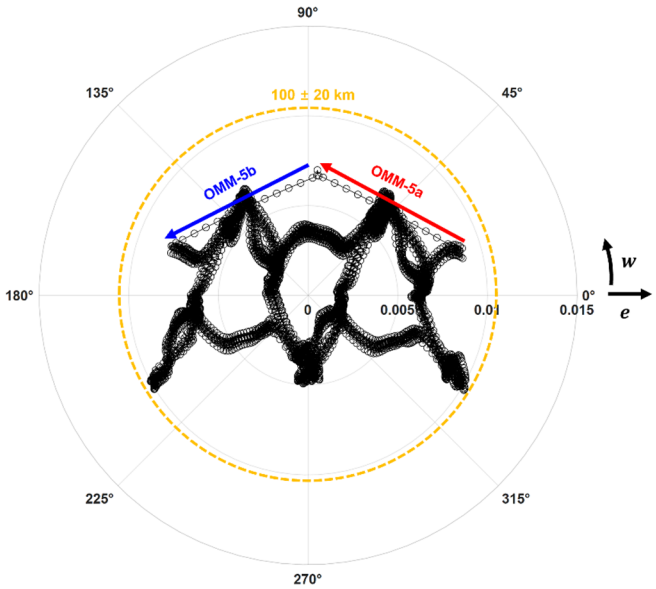


Figure 3. Example of the *e*-*ω* polar plot for the 5th Orbital Maintenance Maneuver (OMM-5), showing altitude dead-band control through paired maneuvers OMM-5a and OMM-5b.

3.2. Orbit Determination for OMM Operations

3.2.1. DSN Tracking

For OD, Danuri relied primarily on radiometric tracking data provided by NASA's DSN. The DSN, consisting of globally distributed antenna complexes in Goldstone (California), Madrid (Spain), and Canberra (Australia), enables continuous tracking coverage and high-precision data acquisition, which are essential for accurate orbit estimation. For

OMM operations, the quality and continuity of DSN tracking data were particularly important because both MP and post-MR depended directly on the estimated spacecraft state. For the Danuri mission, the Goldstone, Madrid, and Canberra DSCCs served as the primary tracking facilities, particularly during OMMs, which are considered mission-critical operations. The high-quality radiometric measurements from the DSN enabled the FD team to achieve the accuracy required for reliable OD and maneuver execution. The utilization of DSN services was made possible through a collaboration between KARI and NASA. This partnership, formalized in 2016, involved the accommodation of NASA's SHC payload onboard Danuri in exchange for DSN navigation support.

Initially, ten DSS antennas were allocated to support the Danuri mission, including both primary and backup assets. For nominal operations, the assigned antennas included DSS-14, DSS-24, and DSS-26 at Goldstone; DSS-34, DSS-36, and DSS-43 at Canberra; and DSS-54, DSS-56, DSS-63, and DSS-65 at Madrid [36]. However, during actual operations, antenna assignments were frequently adjusted due to competing mission priorities, launch schedules, contingency events, and occasional antenna anomalies. Despite these variations, efforts were made to retain the originally allocated antennas for mission-critical events such as OMMs. For each OMM, four to six DSS antennas across the three DSCCs were scheduled to provide near-continuous tracking coverage for approximately 48 h before and after maneuver execution. Table 2 summarizes the distribution of antenna support for Danuri's OMMs, categorized by DSCC. Although the actual antenna usage differed from the initial allocation, sufficient DSN tracking coverage was maintained during OMM-critical periods to support reliable OD and maneuver execution.

Table 2. Distribution of DSCC antenna support for Danuri's OMMs, 48 h before and after each maneuver.

DSCC	Station Allocated		Actual Station Used
	Primary	Back-Up	
Goldstone	DSS-24, DSS-26	DSS-14	DSS-24, DSS-26,
Canberra	DSS-34, DSS-36	DSS-43	DSS-34, DSS-36
Madrid	DSS-54, DSS-56, DSS-65	DSS-63	DSS-54, DSS-56, DSS-65

3.2.2. Tracking Data and Arc

For Danuri's OD, radiometric tracking data provided by the DSN were delivered in two formats: the DSN TRK-2-34 and the DSN TDM. Both formats include Sequential Ranging measurements and TCP Doppler data [36]. Although the FDS was capable of processing both formats, the TRK-2-34 format was primarily used for OD due to its compatibility with operational workflows. Two OD solutions were generated prior to each OMM: a preliminary OD and a final OD. The preliminary OD used tracking data up to approximately 48 h before the TIG, whereas the final OD incorporated data up to approximately 24 h prior to TIG. In both cases, the tracking arc length was approximately four days. Accordingly, the preliminary OD used data spanning from 144 to 48 h before TIG, while the final OD used data from 120 to 24 h prior to TIG. This selection of tracking arcs was based on pre-launch OD performance analyses [37,38], which demonstrated that a four-day arc provides sufficiently stable and reliable state estimation for OMM planning. Actually, pre-launch studies for Danuri investigated the effects of tracking-arc length [37], ground tracking support conditions [38], and lunar gravity model selection and truncation level [39] on OD performance. These simulation studies provided a technical basis for developing Danuri's operational OD strategy and selecting the tracking arcs and gravity-model settings used during flight operations. Readers may refer to these studies for detailed analyses of the effects of tracking and gravity-model settings on OD performance.

https://doi.org/10.3390/aerospace13121107

During the 48 h period before and after each OMM, payload operations were minimized to prioritize maneuver execution and ensure high-quality tracking data. This operational constraint was necessary because even small attitude reorientations can introduce significant noise into DSN radiometric measurements, particularly in Doppler data. In addition, during the OD and MP phases preceding each OMM, momentum dumping activities, which are routine operations involving small thruster firings to unload accumulated angular momentum, were carefully reviewed and, if necessary, rescheduled in coordination with the DSN tracking schedule. This ensured that such activities did not interfere with tracking data quality and degrade OD and MP performance. Figure 4 presents the OMM operational timeline for Danuri, including the preliminary and final OD phases with their respective tracking arcs, as well as the post-maneuver OD process.

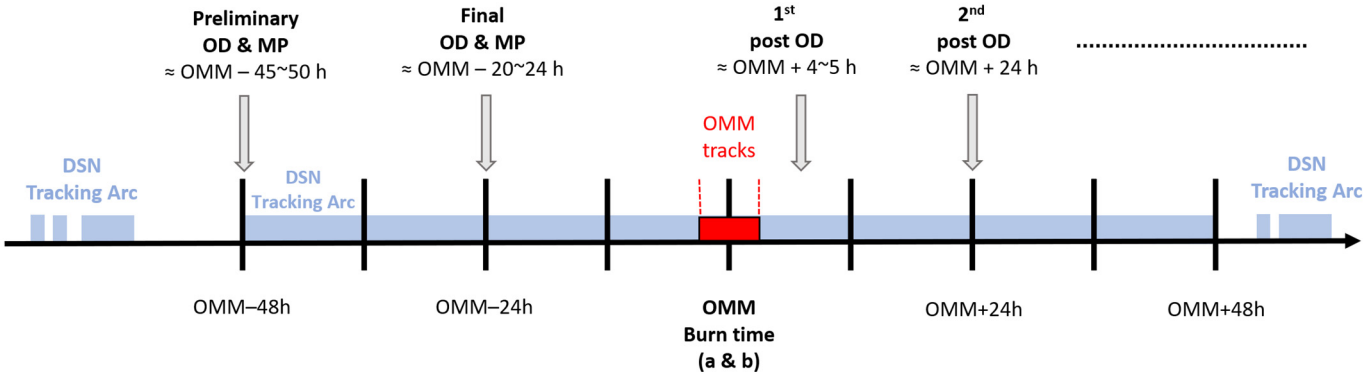


Figure 4. OMM timeline for Danuri's OMM execution. The figure illustrates the tracking arc allocation for preliminary and final OD before OMM execution, as well as the post-OMM OD.

3.2.3. OD Dynamic Model and Estimation Settings

The estimation process for Danuri's OMM operations employed a sequential estimation approach consisting of an extended Kalman filter and a fixed-point backward smoother, which enabled rapid and stable OD solution generation within the operational timeline for OMM planning. The DSN range and Doppler observables were processed to estimate the spacecraft state before and after each maneuver. The OD dynamic model included the non-uniform lunar gravity field, third-body perturbations from the Earth and the Sun, and solar radiation pressure. For the lunar gravity field, the GL0660B model with degree and order 100 × 100 was used for routine operational OD. A separately generated high-fidelity OD solution using GL0660B with degree and order 250 × 250 was used as the reference solution for MR, as described in Section 3.3. These configurations were selected based on analyses conducted before Danuri's launch [39] and operational requirements, balancing modeling fidelity with processing time. The 100 × 100 configuration met routine OD requirements within the operational timeline, while post-processing allowed 250 × 250 for the MR reference solution. This choice was further supported by early operational experience, which suggested that burn execution errors and thrust-efficiency variations were the main contributors to differences between planned and reconstructed delta-V, with gravity-field truncation playing a minor role.

The measurement model included two-way radiometric range and Doppler modeling, tropospheric and ionospheric delay corrections, ground-station plate motion and antenna corrections, and transponder and measurement bias estimation. The primary estimated parameters consisted of Danuri's position and velocity, solar radiation pressure coefficient, transponder bias, and selected station- or measurement-dependent bias terms. Within this estimation framework, potential systematic errors were addressed as follows.

For transponder bias, a bias parameter was estimated for each OD solution. The estimated bias and its associated white-noise level were 4869 ns and 10 ns, respectively. For station errors, the DSN station coordinates were expressed in the ITRF93 reference frame. Their centimeter-level uncertainties were considered negligible compared with the meter-level OD uncertainties reported in this study. Regarding gravitational field model errors, at Danuri's orbital altitude of approximately 100 km, the errors associated with the GRAIL-derived GL0660B model were considered small compared with the effects of model truncation. The truncation effects were quantitatively analyzed in the pre-launch study reported in Ref. [39], which provided guidance for selecting the operational gravity-model settings. Regarding unmodeled accelerations and force-model uncertainties, momentum-dumping events, SRP modeling, and lunar gravity model uncertainties were identified as more significant error sources for Danuri. Accordingly, momentum-dumping activities were scheduled to avoid interference with OMM operations, and the SRP coefficient was estimated as part of the OD process. The position and velocity uncertainties reported in this study are expressed as 3σ 3D RMS values computed from the estimated covariance in the RIC frame.

For OMM operations, the solve-for parameter and filter/smoother settings were selected conservatively to obtain a robust pre-maneuver state estimate rather than to over-parameterize the OD solution. Tracking data were screened through pass-level residual inspection, and data segments affected by station anomalies, short tracking gaps, or non-nominal operational conditions were excluded when necessary. The solve-for parameter set was selected conservatively according to tracking coverage, residual behavior, and solution stability, because the OD result had to be delivered within a limited operational timeline for MP and command generation. Table 3 summarizes the dynamic model and estimation settings used for OMM operations.

Table 3. Summary of OD model and estimation settings for Danuri's OMM operations.

Category	Applied Setting
Estimation method	Extended Kalman filter and a fixed-point backward smoother
Tracking data screening	Pass-level residual inspection and outlier removal
Tracking data	DSN two-way sequential range and TCP Doppler
Tracking data format	TRK-2-34 primarily used, TDM also delivered as a DSN tracking data product
Tracking arc	Preliminary, final, and post-OMM tracking arcs selected according to OD performance and the OMM operational timeline
Primary solve-for parameters	Spacecraft position and velocity at the OD epoch, SRP coefficient, transponder bias, and selected station- or measurement-dependent bias terms
Gravity model	GL0660B: degree and order 100 × 100 for operational OD and 250 × 250 for the refined OD solution used as the MR reference
Other dynamic models	Earth/Sun third-body perturbations, spherical SRP model, and JPL DE430 planetary ephemeris
Measurement model	Two-way radiometric range and Doppler model, tropospheric and ionospheric delay corrections, station plate-motion and antenna corrections, transponder bias, and measurement/time bias estimation
Numerical integrator	RK78 variable-step integrator

Within the OMM timeline, the preliminary OD provided an early state estimate for initial MP, whereas the final OD incorporated more recent tracking data and was used for final maneuver command generation. After OMM execution, post-OMM OD was performed using newly acquired DSN tracking data to reconstruct the achieved orbit. When an OMM was included in the post-maneuver OD arc, maneuver estimation was performed as part of the sequential OD process, using the final planned maneuver information as the initial values of the maneuver components. The resulting estimated delta-V was used for the preliminary OD-based maneuver-performance assessment and subsequent MR analysis.

3.3. Maneuver Recovery

In addition to OD-based estimation, MR was employed to further evaluate maneuver performance. The primary distinction between OD and MR lies in thrust modeling fidelity. While the OD-based estimate was obtained through maneuver estimation within the sequential OD process, MR reconstructs the executed maneuver using detailed thruster modeling and a targeter-based approach. This targeting process can be conceptually expressed as

$$\mathrm{X}_{MR}^{Pre}(t_f;\,\eta)\;-\;\mathrm{X}_{OD}^{Post}(t_f)\;=\;0 \tag{5}$$

where η is the thrust-efficiency scale factor. $\mathrm{X}_{MR}^{Pre}(t_f;\,\eta)$ denotes the selected constraint vector obtained by propagating the state extracted from the post-OMM OD solution at the pre-burn epoch. In this propagation, the detailed maneuver model is applied from the OMM burn start time, and the thrust-efficiency scale factor η is adjusted by the targeter. $\mathrm{X}_{OD}^{Post}(t_f)$ denotes the corresponding constraint vector obtained by propagating the state extracted from the post-OMM OD solution at the post-burn epoch. To provide a higher-fidelity reference for MR, the post-OMM OD solution used in the recovery analysis was generated using the GL0660B lunar gravity model with degree and order 250 × 250, rather than the 100 × 100 model used for routine operational OD. Therefore, the MR targeter adjusts η until the selected constraints of the maneuver-propagated recovery orbit converge to those of the post-OD-derived reference orbit at the final propagation time t_f. Depending on the recovery configuration, the selected constraints may be defined using Keplerian orbital elements, radial, in-track, and cross-track components, or Cartesian state components. Among these constraint sets, two equality-constraint sets were primarily used during operations to compare the recovery and reference trajectories: (1) the radial, in-track, and cross-track position differences; and (2) the differences in the Keplerian elements (a, e, i, Ω, ω). For the orbital-element constraint set, true anomaly was excluded to reduce coupling between along-track phase offsets associated with burn-timing errors and efficiency estimation. With η as the single control parameter, the constraints within each set were solved simultaneously in a least-squares sense. For each OMM, spacecraft telemetry was first used to verify that the burn starts time, duration, and attitude remained within mission requirements. The propagation duration t_f was varied from several hours to several days to assess the consistency of the recovered maneuver performance over different recovery arcs. For Danuri, MR analysis was performed using multiple independent targeter configurations, and the thrust-efficiency values obtained from the converged cases were averaged and used as the representative MR-based estimate of maneuver performance.

3.4. OMM Operational Workflow

3.4.1. Utilization of TDS and FDS

To support the design, planning, execution and post evaluation of OMMs during flight operations, the Danuri FD team designed, developed, validated and utilized the

TDS and the FDS, both components of the KDGS. These systems are based on simulation engines from STK and ODTK from Ansys [40,41]. The TDS and FDS were operated as complementary FD ground systems with distinct roles. In the OMM planning process, the TDS was primarily responsible for reference-orbit design and updates, trajectory-status monitoring, maneuver-schedule generation, and preparation of operational or contingency template scenarios. The FDS then refined these design-level products into operationally executable burn plans by performing MP with detailed thruster modeling, operational OD and parameter estimation, state prediction, fuel accounting, orbit review and confirmation, maneuver command-generation support, and post-maneuver performance assessment. The main interfaces between the two systems included template scenarios, OD and MP products, predictive and definitive ephemerides, fuel and thrust-efficiency estimates, and maneuver confirmation products. This separation allowed design-level maneuver solutions to be refined into operationally executable burn plans while maintaining consistency between the reference trajectory and flight operation products.

3.4.2. Targeting Parameters and Constraints for Executable Maneuver Plans

To translate orbit maintenance strategy into executable maneuver plans, a phased targeting approach was applied across the design, planning, and execution phases, in which the control parameters and constraints were gradually refined to satisfy the altitude dead band derived from the e–ω analysis. During the design phase, control parameters such as TA and finite burn duration were defined for both maneuvers, with thruster directions set to velocity-forward for OMMa and anti-velocity for OMMb. Equality constraints, including periapsis and apoapsis altitudes and the argument of periapsis, were imposed at a LLAN of 270 degrees. Based on the resulting reference orbit, detailed maneuver plans were generated.

In the planning phase, additional control variables, such as azimuth direction, were introduced, and constraints were further refined to tighten the dead-band limits. During execution within the FDS, the elevation direction was incorporated as an additional control parameter to ensure rapid and stable convergence under real-flight conditions. This hierarchical refinement of control parameters enabled the FD team to maintain consistency between the design-level reference trajectory and the executable maneuver solution, thereby supporting robust and reliable OMM design, planning, and execution throughout the mission.

3.4.3. Operational Sequence and IV&V

Using the TDS and FDS, OMM operations were successfully conducted throughout the two-year flight operation period and have continued during the extended mission. For Danuri, OMM MP generally consisted of two stages: a preliminary MP followed by a final MP. Figure 5 illustrates the overall workflow for OMM operations. As shown in Figure 5, the OMM operational procedure follows a cyclic sequence of preliminary and final activity sets. Each activity set includes OD, orbit update, MP, and orbit review and confirmation. In general, two such activity sets are sufficient to complete the OMM design and planning process prior to maneuver execution. After the final MP was confirmed, maneuver commands were generated and uploaded for execution based on the planned burn parameters. Post-maneuver operations differ slightly from the pre-maneuver process, incorporating additional steps such as MR and thruster performance assessment. Because Danuri did not have an onboard accelerometer, the actual maneuver performance could not be directly measured during burn execution. Therefore, post-OMM OD was performed to reconstruct the achieved orbit and estimate the effective thrust efficiency using both the OD results and MR. Within this workflow, the TDS is primarily responsible for orbit updates, while the FDS supports OD, orbit review and confirmation, and maneuver

execution-related activities. The estimated thrust efficiency was then updated and reflected in subsequent MP, forming a closed-loop operational process for repeated OMM execution throughout the mission.

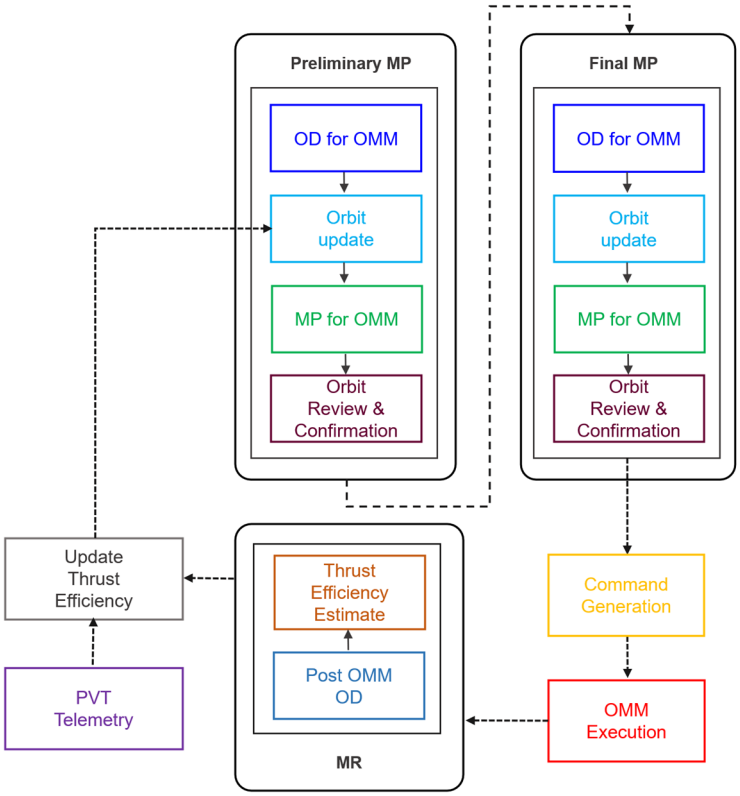


Figure 5. General OMM operational workflow for Danuri.

To improve operational reliability, the Danuri FD team collaborated with the FOD at NASA JSC to perform IV&V in support of OMM execution. This collaboration provided an independent cross-check of the OD and MP results generated by the Danuri FD team, thereby reducing operational risk during mission-critical maneuver activities [42]. This IV&V process was applied not only to OMMs but also to other critical maneuvers conducted during the lunar transfer and orbit insertion phases. NASA JSC FOD used the same DSN tracking data as the Danuri FD team and performed independent OD analyses using its own flight dynamics software. Although the same radiometric tracking data were used, the independent processing environment allowed the resulting OD solutions and maneuver plans to be compared from different operational perspectives. To ensure consistency and maximize accuracy, the Danuri FD team provided detailed maneuver-related information, including planned maneuver parameters and momentum dumping status. Comparative analysis of the independently generated OD solutions and maneuver plans enabled cross-validation of results and identification of discrepancies. This process contributed to refining both OD solutions and MP, thereby enhancing the robustness and reliability of OMM execution.

4. Flight Results

This section presents the results of the 13 OMMs performed by Danuri over a two-year operational period to maintain its mission orbit. The analysis focuses on OD performance before and after each maneuver, as well as the consistency between planned and executed maneuver performance. These results provide a flight-based assessment of how

a low lunar orbiter can maintain a tightly constrained mission orbit using ground-based tracking, OD, and MR, even without onboard acceleration measurements.

4.1. Orbit Determination Performance and Tracking-Arc Assessment

Figure 6 summarizes the 3σ 3D RMS position and velocity uncertainties for each OMM. The preliminary OD solutions were generated using DSN tracking data up to approximately 48 h before the TIG, while the final OD solutions incorporated data up to approximately 24 h prior to TIG. Although final OD solutions are expected to outperform preliminary solutions due to the inclusion of more recent and densely sampled tracking data, this trend was not consistently observed in real flight operations. As shown in Figure 6, this expected improvement was observed in several OMMs, most notably OMM-9, whereas small-to-moderate increases in uncertainty were observed in some cases. This is because the quality of radiometric tracking data can vary depending on antenna availability, tracking geometry, pass duration, and measurement noise characteristics. Occasional inconsistencies or degradation in tracking data quality can therefore limit the improvement of the final OD solution. In addition, external factors such as antenna availability and tracking conditions can introduce unexpected degradation in data quality. Nevertheless, all final OD solutions maintained sufficiently low uncertainty for final MP and execution. To complement the covariance-based uncertainty assessment presented above, the Danuri FD team also checked the consistency of daily OD solutions by comparing positions over overlapping orbit arcs. Additional checks were performed through comparisons with independently generated NASA JSC FOD solutions, as described in Section 3.4.3. These comparisons helped identify discrepancies between solutions and monitor potential systematic errors.

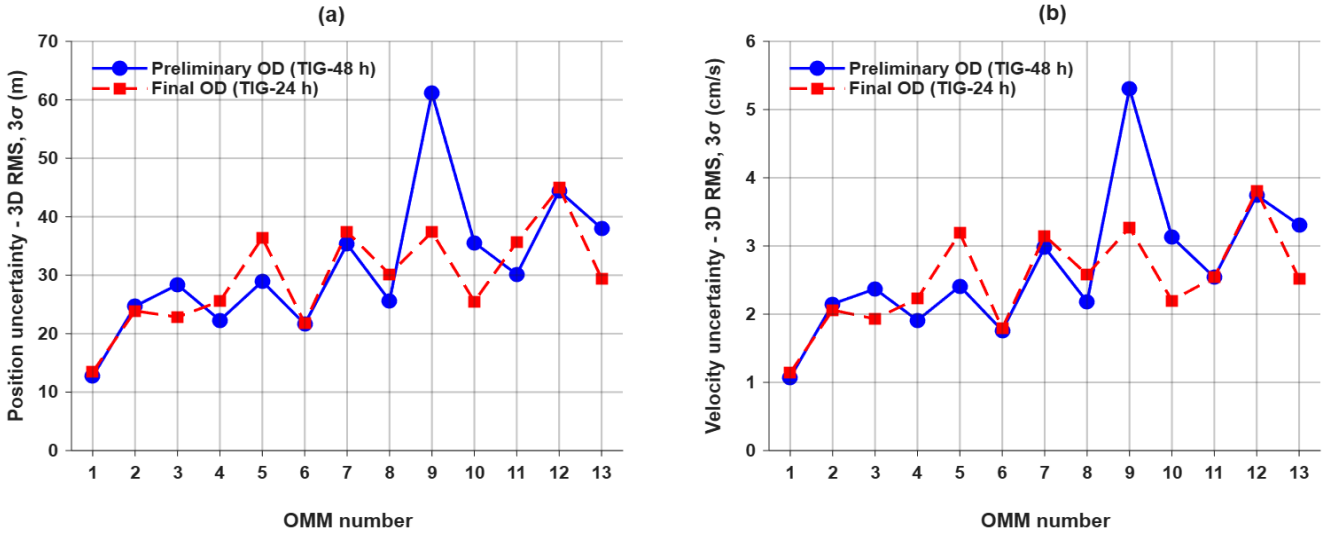


Figure 6. OD uncertainties for the 13 OMMs. (**a**) Three-dimensional position uncertainty and (**b**) three-dimensional velocity uncertainty for the preliminary and final OD solutions.

For the preliminary OD, position uncertainties ranged from 12.69 m to 61.16 m, with the largest value observed for OMM-9 due to a failure of DSS-65 during the planning phase. Velocity uncertainties ranged from 1.07 cm/s to 5.31 cm/s. In the final OD of OMM-9, both position and velocity uncertainties returned to levels comparable to other OMM cases, primarily due to the availability of densely collected high-quality tracking data within the 48–24 h window prior to TIG. The OMM-9 case highlights the importance of dense tracking coverage and high-quality data in maintaining OD accuracy under degraded conditions. However, such cases represent exceptional circumstances. For most OMMs conducted under nominal conditions, the differences between preliminary and

final OD performance remained within comparable ranges. In all cases, the achieved OD accuracy satisfied mission requirements, indicating that both preliminary and final OD solutions were adequate for operational use.

Table 4 presents the post-maneuver OD uncertainty (3D RMS, 3σ) for each OMM. For each maneuver, multiple OD solutions were generated using progressively increasing amounts of post-TIG tracking data: (1) approximately 4~5 h after TIG, (2) up to ~24 h after TIG, and (3) up to 2~3 days after TIG. The results shown in Table 4 correspond to OD#2, for which the final tracking epoch occurred approximately 18–28 h after TIG. As shown in Table 4, post-OMM OD uncertainties were generally on the order of several tens of meters in position and several centimeters per second in velocity, which are significantly better than pre-launch expectations. Position uncertainties ranged from 17.88 m (OMM-1) to 40.47 m (OMM-13), while velocity uncertainties ranged from 2.18 cm/s (OMM-1) to 5.91 cm/s (OMM-13), following a similar trend. The relatively larger uncertainties observed for OMM-13 are likely attributable to a combination of factors, including tracking data quality variations and OD tuning adjustments. However, these uncertainties remained within acceptable limits and did not affect maneuver recovery performance. At a similar orbital altitude, Chang'E-2 reported orbit-overlap differences of 26–63 m in position and 0.02–0.06 m/s in velocity during its 100 × 100 km lunar-orbit phase [43]. These results were obtained using USB and VLBI tracking data, with approximately 14 h tracking arcs and 2 h overlaps. Although the Chang'E-2 results do not separately report OD performance before and after OMMs, their numerical values are of a similar order of magnitude to Danuri's covariance-based OD uncertainties presented in this section, despite the different assessment metrics.

An important operational insight from Table 4 is the selection of tracking arc length for post-OMM OD. Initially, due to limited operational experience, approximately 6~8 days of tracking data prior to TIG were used to ensure sufficient accuracy, based on practices from lunar transfer phase operations. However, as processing large datasets increased computational burden, the FD team reassessed the trade-off between tracking arc length and OD performance. Starting from OMM-6 it was confirmed that using approximately 3~4 days of pre-TIG tracking data yielded comparable OD accuracy. This adjustment significantly reduced processing time and operator workload, while enabling more timely planning of subsequent science operations. For missions with similar orbital characteristics and DSN tracking support, these results suggest that dense DSN tracking coverage extending approximately 48 h before and after maneuver execution may provide sufficient OD performance for operational purposes.

Table 4. OD position and velocity uncertainty (3D RMS, 3σ) achieved after each OMM execution, using OD arcs with final tracking epochs approximately 18–28 h after TIG.

Mnvr.	Pos. Uncertainty (m)	Vel. Uncertainty (cm/s)	Time of First and Last Point of Tracking Data (UTC)	Time of Each OMMa Burn Start (UTC)
OMM-1	17.89	2.18	2023-03-02 00:02:10, 2023-03-09 20:39:55	2023-03-08 23:59:01
OMM-2	26.69	2.95	2023-05-03 00:06:40, 2023-05-11 22:26:14	2023-05-11 00:05:34
OMM-3	24.28	2.51	2023-06-22 01:02:02, 2023-06-29 00:14:54	2023-06-28 02:28:47
OMM-4	22.03	2.58	2023-08-17 07:42:13, 2023-08-24 01:36:43	2023-08-23 00:07:08
OMM-5	22.71	2.50	2023-10-12 06:28:12, 2023-10-18 01:39:02	2023-10-17 01:52:37
OMM-6	27.38	3.04	2023-12-04 00:00:02, 2023-12-07 22:44:01	2023-12-06 23:18:40
OMM-7	37.56	5.21	2024-01-28 00:00:24, 2024-01-31 20:44:54	2024-01-31 00:01:19
OMM-8	22.34	2.62	2024-03-24 00:00:03, 2024-03-28 00:32:43	2024-03-27 01:12:23
OMM-9	21.35	2.45	2024-05-19 00:12:47, 2024-05-23 00:35:22	2024-05-21 20:31:09
OMM-10	24.96	3.03	2024-07-14 00:42:03, 2024-07-17 23:59:01	2024-07-17 01:38:08

OMM-11	34.80	3.60	2024-09-01 00:22:02, 2024-09-04 23:22:07	2024-09-04 00:02:26
OMM-12	30.25	3.45	2024-10-27 09:12:02, 2024-10-30 20:45:02	2024-10-30 01:16:49
OMM-13	40.47	5.91	2024-12-16 02:02:02, 2024-12-20 00:30:31	2024-12-19 01:19:12

4.2. Maneuver Planning Results and Delta-V Characteristics

Danuri's OMMs were primarily designed to maintain the required altitude dead band of the mission orbit. In actual flight operations, however, some OMM plans also had to accommodate additional operational constraints, including conjunction-risk mitigation with other lunar orbiters. Accordingly, this subsection presents the MP results by dividing them into two categories: nominal orbit-maintenance planning and MP under conjunction-related operational constraints.

4.2.1. Nominal Orbit-Maintenance Planning Results

In the nominal orbit-maintenance planning process, the primary objective of MP was to generate executable paired-burn commands for maintaining the required altitude dead band of the mission orbit. Accordingly, the burn start time, delta-V magnitude, and assumed thruster efficiency had to be determined in a manner consistent with the latest OD solution, spacecraft bus operational constraints, and the operational timeline.

As described previously, each OMM was designed through a two-stage MP process, consisting of preliminary and final solutions. Each OMM consisted of paired maneuvers, labeled OMMa and OMMb, typically separated by approximately one hour. Following the final MP stage, maneuver commands were generated and uploaded to the spacecraft after a comprehensive verification process. This process included IV&V with NASA JSC FOD, focusing on the consistency of OD and MP results, as well as additional checks to ensure compliance with spacecraft bus operational constraints. The preliminary MP provided an early maneuver solution for operational preparation, whereas the final MP incorporated the latest OD update and served as the basis for command generation. The resulting preliminary and final MP solutions for all 13 OMMs are summarized in Table 5, including burn start times, delta-V magnitudes, and assumed thruster efficiency values.

Table 5. Preliminary and final planning results for each OMM execution, including burn start times, delta-V magnitudes, and efficiency values.

Mnvr.	Burn Start Time (UTC)		Delta-V (m/s)		Efficiency Assumed
	Preliminary	Final	Preliminary	Final	
OMM-1a	2023-03-08 23:59:02	2023-03-08 23:59:01	7.274	7.274	1.000
OMM-1b	2023-03-09 01:16:44	2023-03-09 01:16:43	7.416	7.416	
OMM-2a	2023-05-11 00:05:35	2023-05-11 00:05:35	7.485	7.485	1.000
OMM-2b	2023-05-11 01:19:00	2023-05-11 01:19:00	7.436	7.436	
OMM-3a	2023-06-28 02:28:47	2023-06-28 02:28:47	2.656	2.656	0.945
OMM-3b	2023-06-28 03:57:47	2023-06-28 03:57:47	8.443	8.443	
OMM-4a	2023-08-23 00:07:08	2023-08-23 00:07:08	6.975	6.975	0.937
OMM-4b	2023-08-23 01:17:49	2023-08-23 01:17:49	7.027	7.027	
OMM-5a	2023-10-17 01:52:35	2023-10-17 01:52:37	6.948	6.948	0.915
OMM-5b	2023-10-17 03:02:15	2023-10-17 03:02:18	6.986	6.986	
OMM-6a	2023-12-06 23:18:34	2023-12-06 23:18:40	6.890	6.877	0.917
OMM-6b	2023-12-07 00:30:49	2023-12-07 00:30:41	6.896	6.896	
OMM-7a	2024-01-31 00:01:28	2024-01-31 00:01:19	8.027	8.027	0.900
OMM-7b	2024-01-31 01:01:36	2024-01-31 01:01:47	12.870	12.882	
OMM-8a	2024-03-27 01:12:23	2024-03-27 01:12:23	7.446	7.446	0.883
OMM-8b	2024-03-27 02:21:33	2024-03-27 02:21:33	6.349	6.355	
OMM-9a	2024-05-21 20:31:09	2024-05-21 20:31:09	6.934	6.935	0.874
OMM-9b	2024-05-21 23:38:30	2024-05-21 23:38:30	6.904	6.910	

OMM-10a	2024-07-17 01:38:08	2024-07-17 01:38:08	6.871	6.871	0.850
OMM-10b	2024-07-17 02:42:30	2024-07-17 02:42:28	6.804	6.804	
OMM-11a	2024-09-04 00:02:27	2024-09-04 00:02:26	6.735	6.735	0.838
OMM-11b	2024-09-04 01:07:32	2024-09-04 01:07:31	6.786	6.786	
OMM-12a	2024-10-30 01:16:48	2024-10-30 01:16:49	6.845	6.845	0.838
OMM-12b	2024-10-30 02:16:34	2024-10-30 02:16:36	6.873	6.878	
OMM-13a	2024-12-19 01:19:11	2024-12-19 01:19:12	6.720	6.720	0.815
OMM-13b	2024-12-19 02:18:26	2024-12-19 02:18:28	6.795	6.795	

The results in Table 5 show that the preliminary and final maneuver plans were generally consistent throughout the two-year operation. As shown in Table 5, the differences between preliminary and final planning results are minimal in terms of burn timing and delta-V. These small discrepancies are primarily attributable to updates in OD solutions used between the preliminary and final MP stages. The close alignment between preliminary and final delta-V values indicates the robustness of the OD performance and the stability of the MP process. The assumed thruster efficiency values were initially set to 1.000 for OMM-1 and OMM-2. As in-flight experience accumulated, these values were refined to better reflect the actual thruster performance in the mission orbit. The effective efficiency was estimated by comparing the planned delta-V, computed from the commanded burn duration and propulsion model, with the achieved delta-V reconstructed from post-maneuver OD and MR results. Propulsion telemetry, including fuel-tank pressure trends and relevant thermal conditions, was also used to interpret the observed performance variations. These updates contributed to improved maneuver accuracy and overall mission efficiency. As shown in Table 1, the Danuri FD team used a fixed nominal thrust of 3.49 N per ACT, scaled by the thrust-efficiency factor, for MP. Danuri's propulsion system operates in blowdown mode, in which tank pressure decreases as propellant is consumed, leading to a reduction in delivered thrust. The factor therefore accounts for this pressure-dependent thrust relative to the fixed nominal value. Figure 7 shows the tank pressure obtained from PVT telemetry at burn start. The pressure decreased from 19.2 bar at OMM-1 to 15.6 bar at OMM-13, a reduction of approximately 18.75%. The corresponding pressure ratio, 15.6/19.2 = 0.813, is close to the assumed thrust-efficiency factor of 0.815 used for OMM-13. This comparison provides first-order support for interpreting the decreasing factor primarily as a consequence of blowdown operation. The decrease in this factor does not, by itself, demonstrate a loss of intrinsic thruster efficiency or a reduction in thruster service life.

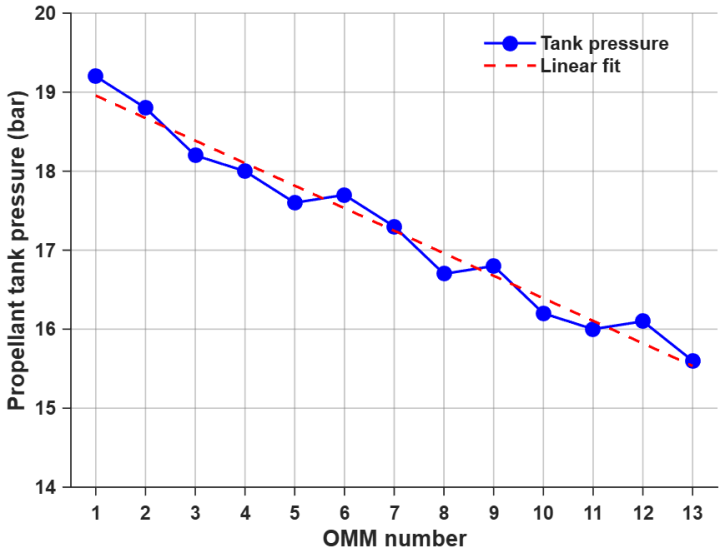


Figure 7. Propellant-tank pressure at burn start for OMM-1 through OMM-13, obtained from PVT telemetry.

Further details on efficiency estimation and updates are provided in Section 4.3, which discusses the MR results. For most OMMs, the required delta-V magnitude was on the order of 6–7 m/s per burn. However, several planning cases deviated from this nominal pattern. OMM-3 and OMM-7 showed clear deviations in delta-V magnitude. In the case of OMM-3, the unequal delta-V allocation between OMM-3a and OMM-3b was introduced to accommodate conjunction-risk-related operational constraints following the CAM. In contrast, the relatively large delta-V of OMM-7 resulted from the inclusion of an inclination-correction objective in addition to altitude maintenance. OMM-7 reduced the orbital inclination by approximately 0.54 degrees, from 90.08 to 89.54 degrees. The post-maneuver inclination was selected so that the average inclination over the following year of operations would satisfy the mean inclination requirement of 90 ± 0.25 degrees. The out-of-plane ΔV component was 15.26 m/s, accounting for approximately 73% of the total ΔV of 20.91 m/s. The inclination correction and eccentricity-vector adjustment were planned together and performed within the same OMM pair. Combining these objectives provided an estimated ΔV saving of more than 8 m/s compared with performing the two corrections separately. Although the delta-V magnitudes of OMM-9 remained comparable to those of nominal OMMs, its burn timing was adjusted to respond to a real-time conjunction-risk constraint during flight operations. The conjunction-related planning adjustments associated with OMM-3 and OMM-9 are discussed separately in Section 4.2.2, because these maneuver plans were influenced by conjunction-risk mitigation requirements rather than nominal altitude maintenance alone.

4.2.2. Maneuver Planning Under Real-Time Conjunction-Risk Constraints

Two conjunction events affected OMM planning in different ways during flight operations. OMM-3 was replanned following the execution of a separate CAM, whereas the timing of OMM-9 was adjusted so that the OMM itself contributed directly to conjunction-risk mitigation. Accordingly, the OMM-3 and OMM-9 results shown in Table 5 reflect two different responses to conjunction risk: replanning of OMM-3 after a separate CAM and direct adjustment of the OMM-9 execution timing for risk mitigation.

To account for conjunction-risk constraints in OMM planning, the Danuri FD team considered not only the collision probability (*Pc*) but also OXD, OXT, CAD, and the CA Epoch. These parameters were provided in reports generated by NASA JPL's MADCAP and NASA JSC's CARDS, which the team received under an agreement between NASA and KARI. This subsection summarizes how these two operational responses affected the corresponding maneuver plans. Readers may refer to Ref. [44] for more details on the decision-making processes and coordination with international stakeholders, including the operational timelines, challenges encountered, and efforts made to ensure timely and effective CAM execution.

Specifically, OMM-3a exhibits a delta-V of only 2.656 m/s. This adjustment was made in response to a collision alert issued by NASA JPL MADCAP [45], which raised a red alarm on 11 June 2023, indicating a potential collision between Danuri and India's CH2O on 24 June 2023. For the conjunction predicted at 06:12:36 UTC on that date, the assessment before mitigation reported a CAD of 17.1 km, an OXD of −0.2 km, and an OXT of 10.7 s. The absolute values of OXD and OXT were below the corresponding MADCAP thresholds of 1.6 km and 17.1 s. Although the initial collision-probability estimates were low, successive reports showed the closest conjunctions shifting to earlier orbital revolutions. Based on this trend and the continuing red alerts, the Danuri FD team decided to execute a separate CAM prior to OMM-3 to mitigate the collision risk. The CAM to avoid CH2O was designed with a delta-V of approximately 6.002 m/s, a start time of 21 June 2023, and an efficiency of 0.976. While it was technically feasible to integrate the collision avoidance function into OMM-3 without a separate CAM, the decision was made to execute a

separate CAM maneuver. This approach allowed additional orbital correction opportunities through the subsequent OMM-3 maneuver if the CAM did not execute as intended. Most importantly, the pre-secured DSN tracking data, covering 48 h before and after OMM-3, were expected to support accurate OD and MR even with the additional CAM execution. Eventually, the CAM was successfully executed, effectively eliminating the collision risk. This strategy not only maintained Danuri's mission-orbit altitude through OMMs but also cleared all MADCAP red alerts by providing substantial spatial separation, with Danuri and CH2O nearly 180 degrees apart around the Moon at the originally predicted closest-approach epoch. The OMM-3a and 3b maneuvers shown in Table 5 represent newly planned maneuvers following the CAM execution. Originally, if the CAM had not been necessary, OMM-3a was planned for execution on 28 June 2023 at 00:53:07 (UTC) with a delta-V of approximately 7.312 m/s, and OMM-3b was planned for 28 June 2023 at 02:07:11 (UTC) with a delta-V of approximately 7.325 m/s.

A similar conjunction risk was identified prior to OMM-9. A MADCAP red alarm was issued on 17 May 2024 indicating a potential collision between Danuri and CH2O, with the predicted conjunction date set for 24 May 2024. For the closer of the two conjunctions initially reported for that date, the predicted closest approach was at 09:03:16 UTC, with a CAD of 14.17 km. The OXD was 0.64 km and the OXT was −9.18 s. Their absolute values were below the corresponding MADCAP thresholds of 1.85 km and 9.84 s. On 19 May 2024, the Danuri FD team began reviewing options to adjust the timing of OMM-9 to mitigate this risk, considering DSN scheduling, bus operational constraints, and other mission requirements. As in the OMM-3 case, a separate CAM maneuver could have been executed; however, analysis concluded that simply adjusting the timing of OMM-9 would sufficiently reduce the collision risk. Consequently, the final maneuver plan moved OMM-9a forward by approximately two orbital periods and OMM-9b by one orbital period from the original schedule. With the revised OMM-9 timing included in the updated ephemeris, the predicted CAD for the May 24 conjunction exceeded 24 km. Both JPL's MADCAP results and JSC's subsequent assessment indicated that these adjustments effectively mitigated the collision risk. As a result, the adjusted OMM-9 plan was approved for execution on Danuri. Initially, OMM-9a was scheduled for execution on 22 May 2024 at 00:27:18 (UTC), and OMM-9b on 22 May 2024 at 01:34:13 (UTC).

Together, these cases demonstrate the operational flexibility of the MP process: an OMM can be replanned following a separate CAM, as in OMM-3, or its execution timing can be adjusted to contribute directly to conjunction-risk mitigation, as in OMM-9. In both cases, the overall orbit-maintenance objective was preserved through coordinated OD, tracking, and MP.

4.3. Maneuver Recovery and Performance Reconstruction

This section describes how Danuri's maneuver performance was reconstructed after execution using post-maneuver radiometric tracking data. Because onboard acceleration measurements were not available during OMM executions, the actual delta-V delivered by each maneuver could not be directly measured from onboard data. Therefore, the maneuver recovery process relied on OD-based preliminary performance estimation, followed by MR-based reconstruction and thrust-efficiency calibration.

4.3.1. Tracking-Arc Configuration for Post-Maneuver OD

For Danuri, the tracking-arc configuration around the TIG was a critical element of the OMM recovery process. A complete pre-maneuver tracking arc was required to reduce uncertainty in the maneuver initial state, whereas a complete early post-maneuver tracking arc was required to support rapid confirmation of the executed maneuver. If either tracking segment was insufficient, the separation between orbit-estimation error and

actual maneuver-execution error could become ambiguous. Therefore, DSN tracking passes before and after each OMM were scheduled in advance as part of the maneuver-planning and recovery timeline.

As described previously, multiple OD solutions were generated after each maneuver: OD#1 was typically generated approximately 4–5 h after TIG based on the first post-maneuver tracking arc, OD#2 used additional tracking data collected over approximately 12–24 h after TIG, and OD#3 incorporated data up to 2–3 days after TIG. Since the differences between OD#2 and OD#3 results were negligible, OD#3 was discontinued after OMM-2. The use of OD#1, OD#2, and OD#3 was intended to evaluate how much post-maneuver tracking duration was practically required for reliable performance assessment. This comparison was operationally important because longer tracking arcs can improve robustness but also delay maneuver-performance confirmation and require additional ground-station resources.

4.3.2. OD-Based Preliminary Maneuver-Performance Estimation

Figure 8a compares the final planned delta-V for each OMM with the delta-V estimates obtained from OD#1 and OD#2, while Figure 8b presents the corresponding maneuver performance percentages. The OD-based maneuver performance shown in Figure 8b was calculated as the ratio of the OD-estimated delta-V to the final planned delta-V, expressed as a percentage. As shown in Figure 8a, the delta-V estimates obtained from OD#1 and OD#2 are nearly identical for most OMMs, indicating strong consistency in OD-based performance evaluation. Although OD#1 was typically available approximately 4–5 h after TIG, the results showed that post-maneuver tracking data collected within approximately 2–4 h after TIG were sufficient to provide a meaningful preliminary maneuver-performance estimate. Given Danuri's orbital period of approximately 1.9 h, this tracking duration corresponds to about one to two orbital periods. These results indicate that the first post-maneuver tracking opportunity can provide a meaningful quick-look assessment of maneuver execution. It should be noted that this finding applies only to OD-based preliminary maneuver-performance assessment under Danuri's tracking conditions, orbital characteristics, and operational requirements. The subsequent OD#2 solution, using additional tracking data over approximately 12–24 h, served as a refined estimate for confirming the OD#1 result and supporting follow-on orbit prediction.

Another key observation from Figure 8b is the improvement in maneuver performance after OMM-2. While OMM-1 and OMM-2 exhibited performance levels of approximately 97%, subsequent maneuvers achieved performance levels of 98–99%. This improvement resulted from in-flight calibration of thruster efficiency. Initially, the efficiency was assumed to be 1.000; however, following early maneuver executions, the FD team refined efficiency estimates using propulsion telemetry data, including fuel tank pressure trends. Accurate efficiency prediction was particularly critical for Danuri, as the spacecraft was not equipped with an onboard accelerometer and maneuver execution relied entirely on pre-defined burn durations. The blowdown operation mode introduced additional complexity, as pressure variations during burns and thermal effects due to solar illumination affected thrust performance. These uncertainties occasionally resulted in slight over-performance ("hot burns") exceeding 100%. Consequently, OD-based performance estimation was not only a post-maneuver diagnostic activity but also an input to the calibration of future MP assumptions.

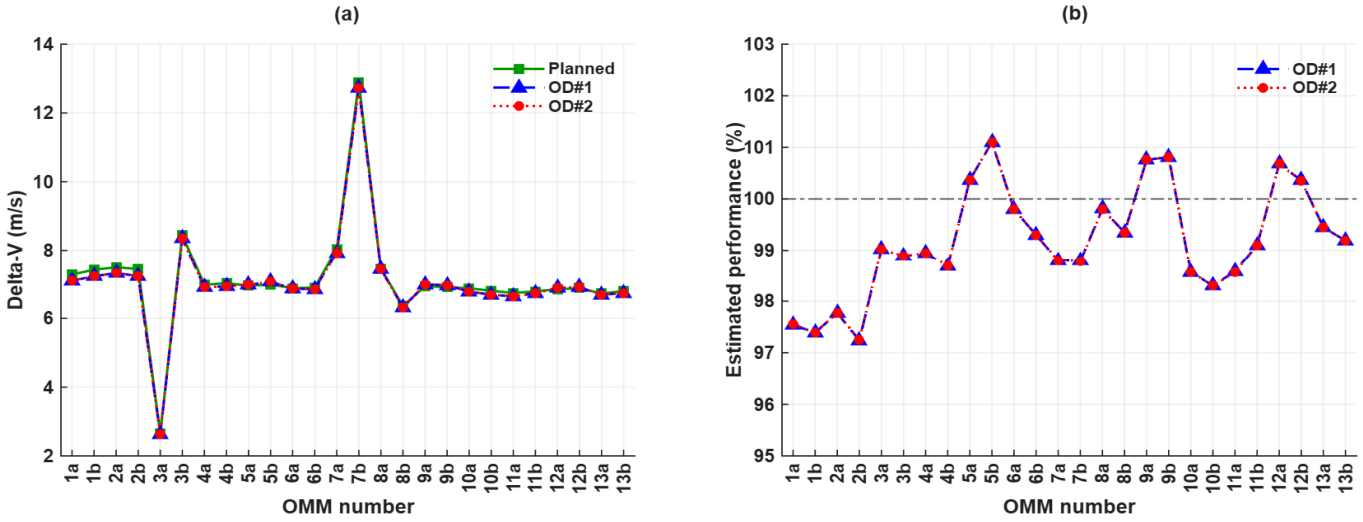


Figure 8. OD-based maneuver-performance estimation for each OMM. (**a**) comparison of the final planned delta-V magnitude with the delta-V estimates obtained from OD#1 and OD#2. (**b**) corresponding maneuver performance estimates obtained from OD#1 and OD#2.

4.3.3. MR-Based Delta-V Reconstruction and Thrust-Efficiency Calibration

While OD-based estimation provided a rapid assessment of the achieved delta-V, MR was used to reconstruct the maneuver more explicitly by considering the thrust model and the efficiency parameter. This distinction is important because OD-based estimates are primarily derived from the orbital change after burn, whereas MR attempts to recover the effective maneuver execution itself. It should be noted that, for the MR analysis, a separate refined post-OMM OD solution was generated using a higher-degree-and-order lunar gravity model than that used for routine operational OD, as summarized in Table 3. This higher-fidelity OD solution was used to provide a more reliable reference orbit for MR and thereby improve the overall robustness of the maneuver reconstruction.

Figure 9 presents the MR results, where the total delta-V for each OMM is evaluated without separating OMMa and OMMb. This approach enables direct comparison between MR-derived efficiency and the efficiency values assumed during MP. While Figure 8 evaluates maneuver performance directly from post-maneuver OD solutions, Figure 9 summarizes the MR-based reconstructed results for all OMM pairs. For Danuri's operations without an onboard accelerometer, three different thrust-efficiency quantities were used, as shown in Figure 9a. In Figure 9a, the "Efficiency Assumed in MP" corresponds to the values used during MP which are shown in the final column of Table 5. The "MR scale factor (Efficiency-1)" represents the efficiency scale factor directly obtained during the MR process, where it was used as a control parameter. The "Calibrated efficiency (Efficiency-2)" is the calibrated thrust efficiency, computed by multiplying the "Efficiency Assumed in MP" value by "MR scale factor (Efficiency-1)". The comparison among these three quantities illustrates how the thrust-efficiency assumption used for MP was progressively calibrated based on the MR results. In Figure 9b, the "Final Planned Delta-V" represents the total planned delta-V combining OMMa and OMMb for each OMM pair, while the "MR-Reconstructed Delta-V" represents the corresponding total delta-V estimated through MR. The "Estimated Maneuver Performance" is calculated by subtracting the absolute percentage difference between the MR-reconstructed and final planned delta-V from 100%. Values close to 100% indicate close agreement with the planned delta-V, whether the reconstructed value is higher or lower. Therefore, the average "Estimated Maneuver Performance" of approximately 99%, shown in Figure 9b, indicates close agreement between the reconstructed and planned Delta-V; it does not mean that the thruster efficiency or the reconstruction accuracy was 99%. Readers should note that the MR

results shown in Figure 9 were evaluated at the OMM-pair level because each orbit-maintenance activity was operationally executed as a paired OMMa/OMMb sequence.

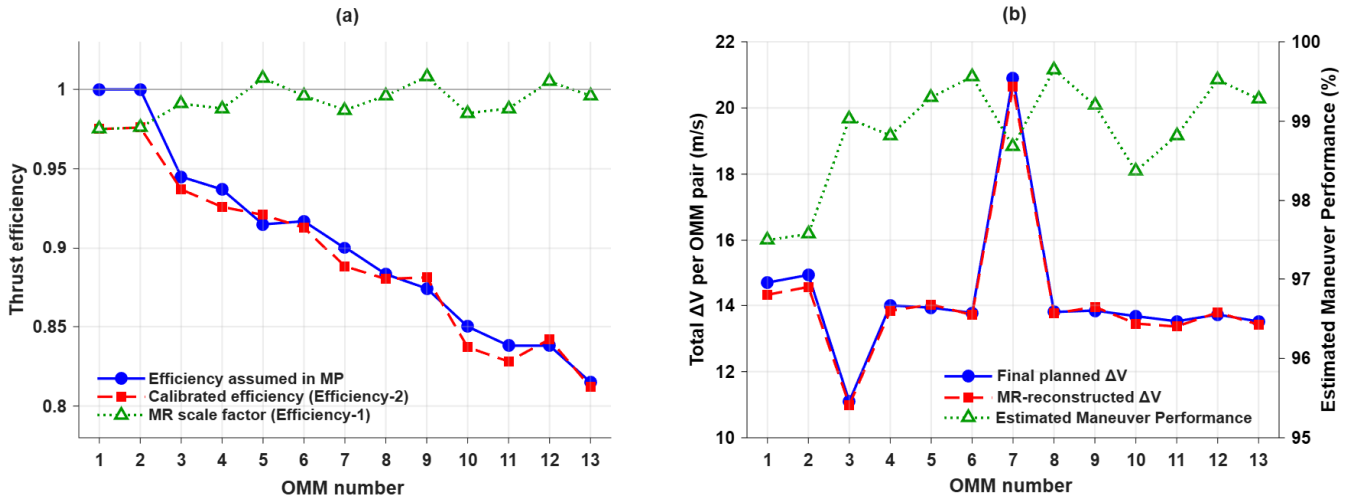


Figure 9. MR-based reconstructed results for the 13 OMM pairs. (**a**) Comparison of assumed, MR scale factor, and calibrated thrust efficiencies. (**b**) Comparison of final planned and MR-reconstructed delta-V with estimated maneuver performance.

When interpreting the MR results shown in Figure 9, the uncertainties involved in the reconstruction process should also be considered. OD errors and tracking geometry affect the reference orbit used for MR, while thrust-model and maneuver-timing uncertainties can influence the estimated scale factor and reconstructed delta-V. During Danuri's real-time flight operations, these contributions were not separately quantified because their individual effects were hard to isolate. Indeed, the influence of burn-direction uncertainty should also be examined to support the MR results. As an example, the thrust-efficiency scale factor for OMM-9 was 1.0080 when only efficiency was adjusted and 1.0063 when burn direction was included as an additional control parameter. The difference of 0.0017 corresponds to approximately 2.4 cm/s when scaled by the OMM-9 pair delta-V of 13.845 m/s. The small change observed in this case supports the use of efficiency-only MR as the baseline.

To summarize the overall maneuver expenditure, the planned and executed Delta-V values for the 13 OMM pairs shown in Figure 8 were combined with those of the three separate CAMs described in detail in Ref. [44]. The cumulative planned and executed Delta-V values over the two-year period were 194.49 m/s and 192.68 m/s, respectively. Nominal orbit maintenance required an average Delta-V of approximately 13.83 m/s per OMM pair. Using this average as a reference, the estimated contributions to the executed Delta-V were 179.83 m/s for orbit maintenance, 6.80 m/s for inclination correction, and 6.05 m/s for conjunction-risk mitigation, including the separate CAMs. Readers should note that this Delta-V breakdown is approximate, as some OMMs combined altitude maintenance with inclination correction or conjunction-risk mitigation.

4.3.4. Consistency Between OD-Based and MR-Based Estimates

Comparison of the pair-level OD-based estimates derived from Figure 7 with the MR-based results shown in Figure 8 confirmed close agreement between the two approaches. The delta-V differences were only on the order of a few cm/s. The maneuver performance estimated through MR ranges from 97.50% to 99.65%, remaining closely consistent with the OD-based estimates. The small differences between the two estimates reflect the more refined thrust modeling and the high-fidelity OD reference solution used in the MR process. Furthermore, the calibrated efficiency values obtained from MR closely track the

efficiency values assumed during MP, demonstrating the effectiveness of the iterative thrust-efficiency calibration process. Danuri's maneuver performance described above can be indirectly compared with the OMM results reported for LADEE. LADEE reported a mean delta-V error of +0.26% and a 3σ dispersion of 3.92% [26]. Danuri's recovered-to-planned delta-V ratios ranged from 97.50% to 99.65%. These results show that Danuri's recovered delta-V closely matched the planned values, supporting the practical effectiveness of the operational workflow presented in this study, including maneuver recovery without onboard acceleration measurements. However, Danuri's values describe the observed range across OMM pairs, whereas LADEE's 3σ value describes the statistical spread of individual OMM errors. Differences in orbital conditions, propulsion systems, and estimation methods should also be considered when interpreting this comparison.

Despite the absence of an onboard accelerometer, Danuri achieved an average maneuver performance of approximately 99%. This level of performance demonstrates the effectiveness of the adopted calibration and operational strategies and was sufficient to maintain the mission orbit without impacting scientific operations. Overall, the results indicate that accurate maneuver performance reconstruction can be achieved without onboard acceleration measurements, provided that high-quality tracking data and robust calibration strategies are available. The close agreement between the OD-based and MR-based estimates confirms that the adopted recovery strategy was sufficient for practical maneuver-performance reconstruction. In particular, the results show that reliable post-maneuver assessment can be achieved without onboard acceleration measurements when early post-TIG tracking data, refined OD solutions, and calibrated thrust-efficiency modeling are used together. These results provide the technical basis for the operational lessons discussed in Section 5, especially the importance of securing pre- and post-maneuver tracking schedules as an integral part of OMM operations.

5. Operational Lessons and Implications

The two-year OMM experience of Danuri provides several practical implications for maintaining a low lunar polar orbit under both nominal and time-varying operational constraints. First, OMM planning should be treated as an adaptive process rather than a fixed periodic station-keeping activity. Although the baseline OMM sequence was designed to maintain the spacecraft within the 100 ± 20 km mission-orbit requirement, actual flight operations showed that maneuver timing and targeting could be affected by late-breaking operational constraints, including conjunction-risk mitigation requirements. Therefore, the MP process should preserve sufficient flexibility to re-optimize the maneuver epoch, target conditions, and delta-V magnitude while still satisfying the primary orbit-maintenance objective.

Second, the planning and securing of OD tracking arcs around each maneuver should be regarded as an essential part of OMM operations. For a low lunar orbiter, the quality of pre- and post-maneuver OD solutions directly determines how reliably the maneuver execution can be assessed. In particular, a full tracking arc immediately before the maneuver is important for reducing uncertainty in the maneuver initial state, whereas an early post-maneuver tracking arc within several hours after TIG is critical for quick reconstruction of the executed delta-V. This was especially important for Danuri because onboard acceleration measurements were not available. Under this condition, post-maneuver radiometric tracking data provided the primary basis for estimating maneuver performance, reconstructing thrust efficiency, and assessing maneuver-execution errors. The Danuri experience also indicates that tracking schedules should be reserved in advance as part of the OMM planning process, rather than treated as a separate ground-operation activity. Securing sufficient tracking coverage before and after TIG enables timely OD, MR, and maneuver-performance assessment. The early post-maneuver solution provides rapid

confirmation of maneuver execution, while additional tracking data over approximately 12–24 h can be used to refine and validate the estimated performance. In contrast, routine extension to multi-day post-maneuver OD arcs may not always be necessary when the differences from the shorter-arc solutions are negligible, as observed in the comparison of the OD-based performance estimates. Therefore, an efficient tracking strategy should balance rapid maneuver assessment, OD accuracy, and ground-station scheduling constraints.

Third, the OD–MP–MR process should be operated as a closed-loop framework. The MP solution depends directly on the latest OD solution and its prediction quality, whereas MR provides post-maneuver reconstruction results that can be used to assess the executed delta-V and update thrust-efficiency assumptions for subsequent maneuvers. This closed-loop use of OD, MP, and MR was particularly important for Danuri because onboard acceleration measurements were not available during most of the OMM operations. The results in Figures 8 and 9 indicate that reliable maneuver-performance estimates can still be obtained from radiometric tracking data when the post-maneuver OD and MR processes are properly configured.

Fourth, an OMM can provide an operational opportunity for conjunction-risk mitigation when the required orbital adjustment is compatible with the orbit-maintenance objective and mission constraints. In the Danuri operations, two OMM cases were affected by real-time conjunction-risk assessments. The two cases demonstrated different forms of operational flexibility. The OMM-9 case showed that an already planned orbit-maintenance maneuver can be rescheduled to reduce conjunction risk, whereas the OMM-3 case demonstrated the need for flexible orbit-maintenance replanning following the execution of a separate CAM. However, this approach requires rapid coordination among flight dynamics analysis, mission operations, and external conjunction-assessment teams, because small changes in maneuver epoch or delta-V direction can affect both the post-maneuver orbit-maintenance condition and the close-approach geometry.

Finally, the Danuri experience emphasizes that future lunar orbit operations will require well-defined international coordination interfaces. During Danuri's conjunction-related OMM adjustments, operational coordination involved KARI and external organizations, including NASA JPL, JSC, GSFC, JAXA, ISRO, and ispace. For future lunar missions, timely exchange of updated ephemerides, covariance information, maneuver plans, and decision timelines will be essential for safe and reliable operations in an increasingly active lunar orbital environment.

6. Conclusions

This study presented the two-year orbit-maintenance and maneuver-recovery results of KPLO, also known as Danuri, in a 100 ± 20 km low lunar polar orbit. During the nominal and first extended mission phases, Danuri successfully executed 13 OMM pairs and maintained the required mission orbit with a mean inclination of 90 ± 0.25 deg. The OMM strategy was implemented using paired maneuvers to control the eccentricity and argument of periapsis, and each maneuver was supported by a two-step planning process consisting of preliminary and final MP. The results confirmed that the combined OD–MP–MR workflow, supported by DSN radiometric tracking and independent IV&V with NASA FOD, provided a reliable operational framework for low lunar orbit maintenance.

The flight results showed that post-maneuver OD uncertainties at the level of several tens of meters in position and several centimeters per second in velocity could be achieved when sufficient DSN tracking data were available before and after maneuver execution. In addition, post-maneuver tracking data collected within approximately 2–4 h after TIG, corresponding to about one to two orbital periods, were sufficient to provide practical preliminary maneuver-performance estimates. However, this finding does not establish a

generally applicable minimum or optimal tracking arc length, as the appropriate arc length depends on each mission's tracking conditions, orbital characteristics, and operational requirements. Because Danuri did not have onboard acceleration measurements available for direct maneuver reconstruction, MR was performed using post-OMM OD solutions, detailed thrust modeling, and targeter-based efficiency estimation. The OD- and MR-based results were consistent, demonstrating that maneuver performance of approximately 99% on average could be achieved through in-flight thrust-efficiency calibration. The operational cases involving conjunction-risk mitigation further showed that OMM planning can be adapted to satisfy real-time safety constraints while preserving orbit-maintenance objectives. These results provide flight-proven guidance for future low lunar orbit missions that require reliable orbit maintenance and maneuver recovery under limited onboard diagnostic capability.

Author Contributions: Conceptualization, J.B. (Jonghee Bae) and Y.-J.S.; writing—original draft preparation, J.B. (Jonghee Bae) and Y.-J.S.; writing—review and editing, J.B. (Jonghee Bae), S.H., J.B. (Jun Bang) and Y.-J.S.; Supervision, J.B. (Jonghee Bae) and Y.-J.S.; Visualization, J.B. (Jonghee Bae), S.H., J.B. (Jun Bang) and Y.-J.S.; Methodology, J.B. (Jonghee Bae), S.H., J.B. (Jun Bang) and Y.-J.S.; Software, J.B. (Jonghee Bae), S.H., J.B. (Jun Bang) and Y.-J.S.; Data curation, J.B. (Jonghee Bae), S.H., J.B. (Jun Bang) and Y.-J.S. All authors have read and agreed to the published version of the manuscript.

Funding: This work was supported by KARI through project No. FR26L01. Y.-J. Song was supported by Global-Learning & Academic research institution for Master's·PhD students, and Postdocs (LAMP) Program of the National Research Foundation of Korea (NRF) grant funded by the Ministry of Education (No. RS-2025-25442355). Also, he was supported by the BK21 FOUR program through National Research Foundation of Korea (NRF) under Ministry of Education (Kyung Hee University, Human Education Team for the Next Generation of Space Exploration).

Data Availability Statement: The data presented in this study may be available on request from the corresponding author. However, due to security and confidentiality considerations, access to the data may be restricted and will be subject to internal review and public release approval by KARI.

Acknowledgments: The authors sincerely thank their colleagues for their important contributions to the success of the Danuri flight operations. They would like to give special thanks to Kara M. Pohlkamp, Shane Fuller, Timothy Stuit, Patrick Zimmerman, Charles Bennett, Jeffery Mauldin, Adrianna Ramirez, Sean McArdle, Partrick Renaud, and Bryan E. Snook from NASA/JSC FOD for their excellent work on IV&V. They also thank Sandy W. Kwan, Sami Asmar, Timothy Pham, Jay Adams, Jeanne Makihara, Kade Peich, and Rylee Mitchell from NASA's DSN team for their reliable tracking support. Finally, the authors express their gratitude to their colleagues at KARI and NASA for their continued support.

Conflicts of Interest: The authors declare no conflicts of interest.

Abbreviations

The following abbreviations are used in this manuscript:

ACT	Attitude Control Thruster
BLT	Ballistic Lunar Transfer
CA	Close Approach
CAD	Close Approach Distance
CAM	Collision Avoidance Maneuver
CARDS	Conjunction Assessment of Risk in Deep Space
CH2O	Chandrayaan-2 Orbiter
DSCC	Deep Space Communications Complex

DSN	Deep Space Network
DSS	Deep Space Station
DTN	Delay-Tolerant Networking
FD	Flight Dynamics
FDS	Flight Dynamics Subsystem
FOD	Flight Operations Directorate
GRAIL	Gravity Recovery and Interior Laboratory
GSFC	Goddard Space Flight Center
Isp	Specific Impulse
ISRO	Indian Space Research Organization
ITRF93	International Terrestrial Reference Frame 1993
IV&V	Independent Validation and Verification
JAXA	Japan Aerospace eXploration Agency
JPL	Jet Propulsion Laboratory
JSC	Johnson Space Center
KARI	Korea Aerospace Research Institute
KDGS	KPLO Deep-Space Ground System
KDSA	Korea Deep Space Antenna
KGRS	KPLO Gamma Ray Spectrometer
KMAG	KPLO Magnetometer
KPDS	KARI Planetary Data System
KPLO	Korea Pathfinder Lunar Orbiter
LADEE	Lunar Atmosphere and Dust Environment Explorer
LLAN	Lunar Longitude of Ascending Node
LLO	Low Lunar Orbit
LOI	Lunar Orbit Insertion
LP	Lunar Prospector
LRO	Lunar Reconnaissance Orbiter
LUTI	Lunar Terrain Imager
MADCAP	Multi-mission Automated Deep-space Conjunction Assessment Process
MP	Maneuver Planning
MR	Maneuver Recovery
NASA	National Aeronautics and Space Administration
OD	Orbit Determination
ODTK	Orbit Determination Tool Kit
OMM	Orbit Maintenance Maneuver
OXD	Orbit Crossing Distance
OXT	Orbit Crossing Time
PI	Principal Investigator
PolCam	Wide-Angle Polarimetric Camera
PVT	Pressure Volume and Temperature
RIC	Radial, In-track, and Cross-track
RK78	Runge–Kutta 7th–8th Order
RMS	Root Mean Square
SELENE	SELenological and Engineering Explorer
SHC	ShadowCam
SLIM	Smart Lander for Investigating Moon
SRP	Solar Radiation Pressure
STK	Systems Tool Kit
TA	True Anomaly
TCP	Total Count Phase
TDM	Tracking Data Message
TDS	Trajectory Design System
TIG	Time of Ignition
TRK-2-34	Tracking System Data Archival Format

https://doi.org/10.3390/aerospace13121107

USB	Unified S-Band
VLBI	Very Long Baseline Interferometry

References

1. Smith, M.; Craig, D.; Herrmann, N.; Mahoney, E.; Krezel, J.; McIntyre, N.; Goodliff, K. The Artemis program: An overview of NASA's activities to return humans to the Moon. In Proceedings of the 2020 IEEE Aerospace Conference, Big Sky, MT, USA, 7–14 March 2020; pp. 1–10. https://doi.org/10.1109/AERO47225.2020.9172323.
2. Ouyang, Z.; Li, C.; Zou, Y.; Zhang, H.; Lü, C.; Liu, J.; Liu, J.; Zuo, W.; Su, Y.; Wen, W.; et al. Primary scientific results of Chang'E-1 lunar mission. *Sci. China Earth Sci.* **2010**, *53*, 1565–1581. https://doi.org/10.1007/s11430-010-4056-2.
3. Wang, Q.; Liu, J. A Chang'e-4 mission concept and vision of future Chinese lunar exploration activities. *Acta Astronaut.* **2016**, *127*, 678–683. https://doi.org/10.1016/j.actaastro.2016.06.024.
4. Zhou, C.; Jia, Y.; Liu, J.; Li, H.; Fan, Y.; Zhang, Z.; Liu, Y.; Jiang, Y.; Zhou, B.; He, Z.; et al. Scientific objectives and payloads of the lunar sample return mission—Chang'E-5. *Adv. Space Res.* **2022**, *69*, 823–836. https://doi.org/10.1016/j.asr.2021.09.001.
5. Mathavaraj, S.; Negi, K.; Vaibhav, G. ISRO's unprecedented journey to the Moon. *Acta Astronaut.* **2020**, *177*, 286–298. https://doi.org/10.1016/j.actaastro.2020.07.046.
6. Ishida, T.; Fukuda, S.; Kariya, K.; Kamata, H.; Takadama, K.; Kojima, H.; Sawai, S.; Sakai, S.-I. Vision-based navigation and obstacle detection flight results in SLIM lunar landing. *Acta Astronaut.* **2025**, *226*, 772–781. https://doi.org/10.1016/j.actaastro.2024.11.002.
7. NASA Space Science Data Coordinated Archive (NSSDCA). Peregrine Mission 1. Available online: https://nssdc.gsfc.nasa.gov/nmc/spacecraft/display.action?id=PEREGRN-1 (accessed on 9 December 2024).
8. Hernando-Ayuso, J.; Gonzalez Meruelo, F.; Sanchez Duran, A.; Monteiro Padovan, T.; Harrison, D.; Marx, A.; Smith, J. Flight dynamics operations for the first ispace lunar lander mission M1. In Proceedings of the 29th International Symposium on Space Flight Dynamics (ISSFD), Darmstadt, Germany, 22–26 April 2024.
9. Aharonson, O.; Russell, C.T.; Head, J.W.; Wieczorek, M.; Garrick-Bethell, I.; Weiss, B.P.; Smith, D.E.; Rowe, K.; Grosz, A.; Amrusi, S.; et al. The science mission of SpaceIL's Beresheet lander. *Planet. Space Sci.* **2020**, *194*, 105115. https://doi.org/10.1016/j.pss.2020.105115.
10. Song, Y.-J.; Bang, J.; Bae, J.; Hong, S.B. Lunar orbit acquisition of the Korea Pathfinder Lunar Orbiter: Design reference vs actual flight results. *Acta Astronaut.* **2023**, *213*, 336–343. https://doi.org/10.1016/j.actaastro.2023.09.021.
11. Bae, J.; Bang, J.; Hong, S.B.; Song, Y.-J. Flight dynamics and trajectory operation in trans-lunar trajectory for Korea lunar orbiter Danuri. *Adv. Space Res.* **2026**, *77*, 2061–2073. https://doi.org/10.1016/j.asr.2025.10.073.
12. Youk, Y.; Ryu, D.; Yoon, J. High-resolution terrain imager development and performance evaluation for lunar exploration. *Appl. Opt.* **2024**, *63*, 221–227. https://doi.org/10.1364/AO.504883.
13. Jeong, M.; Choi, Y.-J.; Kang, K.-I.; Moon, B.; Gu, B.; Kim, S.; Sim, C.K.; Lee, D.; Shkuratov, Y.G.; Videen, G.; et al. Preflight calibration results of Wide-Angle Polarimetric Camera (PolCam) onboard Korean Lunar Orbiter, Danuri. *J. Korean Astron. Soc.* **2023**, *56*, 293–299. https://doi.org/10.5303/JKAS.2023.56.2.293.
14. Robinson, M.S.; Brylow, S.M.; Caplinger, M.A.; Carter, L.M.; Clark, M.J.; Denevi, B.W.; Estes, N.M.; Humm, D.C.; Mahanti, P.; Peckham, D.A.; et al. ShadowCam instrument and investigation overview. *J. Astron. Space Sci.* **2023**, *40*, 149–171. https://doi.org/10.5140/JASS.2023.40.4.149.
15. Lee, J.; Jin, H.; Kim, K.-H.; Park, H.; Jo, W.; Jang, Y.; Kang, H.; Kim, E.; Choi, Y.-J. Correction of spacecraft magnetic field noise: Initial Korea Pathfinder Lunar Orbiter MAGnetometer observation in solar wind. *Sensors* **2023**, *23*, 9428. https://doi.org/10.3390/s23239428.
16. Kim, S.; Kim, K.-J. KPLO gamma-ray spectrometer (KGRS) data processing with Python. *J. Korean Phys. Soc.* **2024**, *84*, 582–589. https://doi.org/10.1007/s40042-024-01036-4.
17. Lee, K.-R.; Jo, J.-H.; Lee, B.-S.; Ji, S. An overview of architecture and applications of delay tolerant network for Korea Pathfinder Lunar Orbiter. In Proceedings of the 27th Asia Pacific Conference on Communications (APCC), Jeju Island, Republic of Korea, 19–21 October 2022; pp. 649–650. https://doi.org/10.1109/APCC55198.2022.9943687.
18. Jeon, M.-J.; Cho, Y.-H.; Kim, E.; Kim, D.-G.; Song, Y.-J.; Hong, S.; Bae, J.; Bang, J.; Yim, J.R.; Kim, D.-K. Korea Pathfinder Lunar Orbiter (KPLO) Operation: From Design to Initial Results. *J. Astron. Space Sci.* **2024**, *41*, 43–60.
19. Folta, D.C.; Beckman, M.; Lozier, D.; Galal, K. Lunar Prospector extended mission. In Proceedings of the 1999 Flight Mechanics Symposium, Greenbelt, MD, USA, 18–20 May 1999; pp. 101–116.

20. Matsumoto, S.; Ogawa, M.; Kawakatsu, Y.; Konishi, H.; Ikeda, H.; Terada, H.; Tanaka, K.; Kato, T.; Otani, K.; Kamikawa, E.; et al. Flight results of Selenological and Engineering Explorer 'KAGUYA' on lunar orbit. In Proceedings of the 21st International Symposium on Space Flight Dynamics, Toulouse, France, 28 September–2 October 2009.
21. Policastri, L.; Carrico, J.P.; Nickel, C.; Kam, A.; Lebois, R.; Sherman, R. Orbit determination and acquisition for LADEE and LLCD mission operations. In Proceedings of the 25th AAS/AIAA Space Flight Mechanics Meeting, Williamsburg, VA, USA, 11–15 January 2015; AAS 15-257.
22. Kam, A.; Plice, L.; Galal, K.; Hawkins, A.; Policastri, L.; Loucks, M.; Carrico, J.P.; Nickel, C.; Lebois, R.; Sherman, R. LADEE flight dynamics: Overview of mission design and operations. In Proceedings of the 25th AAS/AIAA Space Flight Mechanics Meeting, Williamsburg, VA, USA, 11–15 January 2015; AAS 15-212.
23. Beckman, M. Mission design for the Lunar Reconnaissance Orbiter. In Proceedings of the 29th Annual AAS Guidance and Control Conference, Breckenridge, CO, USA, 2007; AAS 07-057.
24. Beckman, M.; Lamb, R. Stationkeeping for the Lunar Reconnaissance Orbiter (LRO). In Proceedings of the 20th International Symposium on Space Flight Dynamics (ISSFD), Annapolis, MD, USA, 24–28 September 2007; Paper 18-3; pp. 1–15.
25. Mesarch, M.; Beckman, M.; Folta, D.C.; Lamb, R.; Richon, K. Maneuver operations results from the Lunar Reconnaissance Orbiter (LRO) mission. In Proceedings of the SpaceOps 2010 Conference, Huntsville, AL, USA, 25–30 April 2010; AIAA 2010-1985. https://doi.org/10.2514/6.2010-1985.
26. Hawkins, A.; Kam, A.; Carrico, J. LADEE Maneuver Planning and Performance. In Proceedings of the 25th AAS/AIAA Space Flight Mechanics Meeting, Williamsburg, VA, USA, 11–15 January 2015; Paper AAS 15-453.
27. Mesarch, M.A. Long-Term Orbit Operations for the Lunar Reconnaissance Orbiter. In Proceedings of the 2023 AAS/AIAA Astrodynamics Specialist Conference, Big Sky, MT, USA, 13–17 August 2023; Paper AAS 23-234.
28. Mukherjee, B.; Anil Kumar, A.K. Current Practices and Future Requirements for Safety of Spaceflight for Missions Beyond Earth's Orbital Regime. In Proceedings of the Second International Orbital Debris Conference, Sugar Land, TX, USA, 4–7 December 2023; Paper 6112.
29. Song, Y.-J.; Hong, S.; Bang, J.; Bae, J.; Jeon, M.-J. The second phase extended mission orbit design for the Korea Pathfinder Lunar Orbiter. *IEEE Access* **2025**, *13*, 85997–86011. https://doi.org/10.1109/ACCESS.2025.3570068.
30. Vallado, D.A. *Fundamentals of Astrodynamics and Applications*, 4th ed.; Microcosm Press: Hawthorne, CA, USA, 2013.
31. Song, Y.-J.; Kim, Y.-R.; Bae, J.; Kim, B.-Y. Evolution of the Selenopotential Model and Its Effects on the Propagation Accuracy of Orbits around the Moon. *Math. Probl. Eng.* **2017**, *2017*, 5493679. https://doi.org/10.1155/2017/5493679.
32. Davis, D.C.; Park, J.-i.; Choi, S.; Whitley, R.; Carrico, J.; Rew, D.-Y.; Choi, S.-W. Enhanced Stationkeeping Maneuver Control Technique for Delta-V Cost Reduction in the Korea Pathfinder Lunar Orbiter. In Proceedings of the 2018 AAS/AIAA Astrodynamics Specialist Conference, Snowbird, UT, USA, 19–23 August 2018.
33. Folta, D.C.; Galal, K.; Lozier, D. Lunar Prospector frozen orbit mission design. In Proceedings of the AIAA/AAS Astrodynamics Specialists Conference, Boston, MA, USA, 10–12 August 1998; AIAA 98-4288. https://doi.org/10.2514/6.1998-4288.
34. Lozier, D.; Galal, K.; Folta, D.C.; Beckman, M. Lunar Prospector mission design and trajectory support. In Proceedings of the AAS/GSFC 13th International Symposium on Space Flight Dynamics, Greenbelt, MD, USA, 11–15 May 1998; AAS 98-323; pp. 297–311.
35. Holt, H.; Yarndley, J.; Armellin, R.; Lara, M.; Bombardelli, C.; Howie, R.; Bland, P. Extremely Low-Altitude Lunar Station Keeping Using Eccentricity Vector Control. In Proceedings of the 29th International Symposium on Space Flight Dynamics, Darmstadt, Germany, 22–26 April 2024.
36. Levesque, M.; Kim, D.G.; Kwan, S.W.; Williams, R.; Long, J.; et al. DSN Mission Event Readiness Review (MERR) for Korea Pathfinder Lunar Orbiter (KPLO) Launch; Internal KARI–JPL Joint Document; KARI/JPL, 2022.
37. Kim, Y.-R.; Song, Y.-J.; Bae, J.; Choi, S.-W. Observational arc-length effect on orbit determination for KPLO using a sequential estimation technique. *J. Astron. Space Sci.* **2018**, *35*, 295–308. https://doi.org/10.5140/JASS.2018.35.4.295.
38. Kim, Y.-R.; Song, Y.-J.; Park, J.-I.; Lee, D.; Bae, J.; Hong, S.B.; Kim, D.-K.; Lee, S.-R. Ground tracking support condition effect on orbit determination for Korea Pathfinder Lunar Orbiter (KPLO) in lunar orbit. *J. Astron. Space Sci.* **2020**, *37*, 237–247. https://doi.org/10.5140/JASS.2020.37.4.237.
39. Kim, Y.-R.; Song, Y.-J.; Bae, J.; Kim, B.-Y. Influence of the Choice of Lunar Gravity Model on Orbit Determination for Lunar Orbiters. *Math. Probl. Eng.* **2018**, *2018*, 5145419. https://doi.org/10.1155/2018/5145419.
40. Ansys. Ansys Systems Tool Kit (STK). Available online: https://www.ansys.com/products/missions/ansys-stk (accessed on 11 December 2024).

41. Song, Y.-J.; Kim, Y.-R.; Bae, J.; Park, J.-I.; Hong, S.; Lee, D.; Kim, D.-K. Overview of the Flight Dynamics Subsystem for Korea Pathfinder Lunar Orbiter Mission. *Aerospace* **2021**, *8*, 222.
42. Song, Y.-J.; Bae, J.; Hong, S.; Bang, J.; Pohlkamp, K.M.; Fuller, S. KARI and NASA JSC collaborative endeavors for joint Korea Pathfinder Lunar Orbiter flight dynamics operations: Architecture, challenges, successes, and lessons learned. *Aerospace* **2023**, *10*, 664. https://doi.org/10.3390/aerospace10080664.
43. Wang, H.; Fan, M.; Dong, G.; Li, H.; Xin, X. Orbital Support for China's Chang'E-2 Lunar Exploration Satellite. In Proceedings of the SpaceOps 2012 Conference, Stockholm, Sweden, 11–15 June 2012.
44. Song, Y.-J.; Hong, S.; Bang, J.; Bae, J.; Jeon, M.-J.; Chung, S.; Fuller, S.; Stuit, T. KPLO's conjunction mitigation in lunar orbit: Operational results and strategic insights from international collaboration. *Acta Astronaut.* **2026**, *241*, 637–653. https://doi.org/10.1016/j.actaastro.2025.11.061.
45. Berry, D. *Conjunction Assessment Process for Lunar Orbiters*; Jet Propulsion Laboratory, California Institute of Technology: Pasadena, CA, USA, 2022. Available online: https://www.nasa.gov/wp-content/uploads/2022/08/moon_conjunction_assess_process-urs309081.pdf (accessed on 16 February 2025).

Disclaimer/Publisher's Note: The statements, opinions and data contained in all publications are solely those of the individual author(s) and contributor(s) and not of MDPI and/or the editor(s). MDPI and/or the editor(s) disclaim responsibility for any injury to people or property resulting from any ideas, methods, instructions or products referred to in the content.